2021

MATURATION OF EQUINE PROXIMAL SESAMOID BONES IN THOROUGHBRED HORSES

Angela Maria Mangine
University of Kentucky, ammangine@gmail.com
Digital Object Identifier: https://doi.org/10.13023/etd.2021.289

STUDENT AGREEMENT:

I represent that my thesis or dissertation and abstract are my original work. Proper attribution has been given to all outside sources. I understand that I am solely responsible for obtaining any needed copyright permissions. I have obtained needed written permission statement(s) from the owner(s) of each third-party copyrighted matter to be included in my work, allowing electronic distribution (if such use is not permitted by the fair use doctrine) which will be submitted to UKnowledge as Additional File.

I hereby grant to The University of Kentucky and its agents the irrevocable, non-exclusive, and royalty-free license to archive and make accessible my work in whole or in part in all forms of media, now or hereafter known. I agree that the document mentioned above may be made available immediately for worldwide access unless an embargo applies.

I retain all other ownership rights to the copyright of my work. I also retain the right to use in future works (such as articles or books) all or part of my work. I understand that I am free to register the copyright to my work.

REVIEW, APPROVAL AND ACCEPTANCE

The document mentioned above has been reviewed and accepted by the student's advisor, on behalf of the advisory committee, and by the Director of Graduate Studies (DGS), on behalf of the program; we verify that this is the final, approved version of the student's thesis including all changes required by the advisory committee. The undersigned agree to abide by the statements above.

Angela Maria Mangine, Student

Dr. James N. MacLeod, Major Professor

Dr. Daniel Howe, Director of Graduate Studies

MATURATION OF EQUINE PROXIMAL SESAMOID BONES IN THOROUGHBRED HORSES

THESIS

A thesis submitted in partial fulfillment of the
requirements for the degree of Master of Science in the
College of Agriculture, Food and Environment
at the University of Kentucky

By

Angela Maria Mangine

Lexington, Kentucky

Director: Dr. James N. MacLeod, Professor of Veterinary Science

Lexington, Kentucky

2021

ABSTRACT OF THESIS

MATURATION OF EQUINE PROXIMAL SESAMOID BONES IN THOROUGHBRED HORSES

Proximal sesamoid bone (PSB) injuries account for approximately 50% of all fatal catastrophic musculoskeletal injuries in Thoroughbred racehorses. In addition, PSB fractures are not uncommon in Thoroughbred foals and yearlings as a result of energetic or intense free exercise. The ability to interpret some PSB pathology assessments, however, is more difficult given the limited information published on the normal development and maturation of these paired sesamoid bones. In addition, the level of normal variation in PSB morphological and structural parameters within the Thoroughbred population as a function of age, body size, gender, and inter-animal variation are not well documented, complicating accurate assessments of PSB pathology.

These knowledge gaps were addressed through postmortem analyses of PSB anatomy from 36 horses representing an age range from birth to skeletal maturity. All study subjects were believed to represent normal appendicular skeletal structure for the Thoroughbred breed and were assessed using clinical computed tomography (cCT) evaluation (n=18 horses, 21 months to six years of age) and micro–computed tomography (μCT) bone morphometry evaluation (n=22 horses, birth to six years of age). Medial PSBs were found to be shorter and deeper with an increased bone mineral density compared to lateral PSBs. Trabecular separation and degree of anisotropy were also greater in medial than lateral PSBs. All of the measured μCT parameters changed with increasing age, clearly documenting a postnatal maturation process. Connectivity density and degree of anisotropy changed rapidly after birth, while the parameters of total volume, bone volume, bone volume fraction, trabecular number, and trabecular thickness changed at a slower rate. Importantly, however, all of these parameters approached a horizontal asymptote before 24 months of age. The only μCT parameter that continued to change beyond two years of age was trabecular separation. These findings greatly advance the understanding of postnatal development and maturation timelines of PSBs in Thoroughbred horses, as well as documenting structural differences between medial and lateral PSBs. The data also indicate that PSBs in Thoroughbred horses have reached skeletal maturity by two years of age, a time that corresponds with the onset of high speed exercise and racing competition. The results define normal structural and morphological characteristics of Thoroughbred PSBs, as well as a preliminary appreciation for the extent of inter-animal variation. This knowledge will provide an essential baseline for the assessment of equine PSB pathologies.

KEYWORDS: Horse, Sesamoid, Maturation, Computed Tomography, Thoroughbred, Bone

Angela Maria Mangine

(Name of Student)

07/27/2021

Date

MATURATION OF EQUINE PROXIMAL SESAMOID BONES IN THOROUGHBRED HORSES

By
Angela Maria Mangine

James N. MacLeod
Director of Thesis

Daniel Howe
Director of Graduate Studies

07/27/2021
Date

DEDICATION

To my nephew, my grandfather, and my godfather.
Forever in my heart

ACKNOWLEDGMENTS

I would first like to acknowledge Dr. James MacLeod for his incredible mentorship throughout my Master's Program. I also want to thank those who are on my committee, Dr. Jennifer Janes and Dr. Emma Adam, for their invaluable insight and support. Additionally, I want to thank my peers, Kathryn Babiarz and Erik Davis, for their tremendous amount of support and understanding. I would not have been able to complete this program or persist through COVID '19 without your constant efforts for our projects and your patience with my fly like attention span. Finally, I want to recognize all of the collaborators on my project, including Dr. Laura Kennedy and the UK Veterinary Diagnostic Lab staff, Dr. Katie Garrett from Rood and Riddle Equine Hospital, Dr. Guigen Zhang from UK Biomedical Engineering, Aviv Brockman from the UK Statistical Consulting Lab, as well as my lab mates, Dr. Bruno Menerim, Dr. ChanHee Mok, Dr. Jasmin Bagge, Sheldon McLetchie, and Grace Camp.

I would be remiss if I did not mention the equally important support I received from family and friends. I would like to thank my friends, Kathryn Bowser and Lauren Hooie, as well as my cousins, Elizabeth and Hannah Vagedes, for forcing me to take time for myself. My husband, Jacob Proctor, provided on-going encouragement throughout the thesis process and through wedding planning during a global pandemic. My parents, Marsha and Bob Mangine, were always there to give me realistic advice and a free meal. Finally, I would like to thank my brothers, A.J., Robert, and Matt; my sisters-in-law, Kim and Amanda; and my nieces and nephew, Sophia, MacKenzie, and Joseph, for always being there when I need a hug or a smile.

TABLE OF CONTENTS

LIST OF TABLES

.

LIST OF FIGURES

CHAPTER 1. INTRODUCTION

1.1 Epidemiology

Catastrophic musculoskeletal injuries (CMI) are a major causes of early career termination and death in Thoroughbred racehorses.[1,2] The Equine Injury Database reports 1.41 racing fatalities per 1000 starts for 2020, which includes all horses that die or are euthanized due to injury at participating racetracks (includes musculoskeletal injuries, non-musculoskeletal injuries, and sudden deaths) during competition.[3] Proximal sesamoid bone (PSB) fractures are the most common site of fracture in racing horses, present in 40% to 50% of CMI horses.[4,5] Chronic apical fractures can be found in both racing horses and sport horses that exhibit little to no lameness and are not uncommonly diagnosed as an incidental finding during imaging studies for other purposes.[6] Proximal sesamoid fractures are also common fatigue injuries in young foals under 2 months of age that experience strenuous exercise, often when running after their dam in pasture.[7] Other PSB pathology, including sesamoiditis, are seen more frequently in immature horses from age 2 months to 2 years.[7]

Despite being a prevalent site of CMI injury in racing horses and a not uncommon site for PSB injury in young horses, there is little known about their normal maturation, structural anatomy, and population variation. The lack of normal, baseline data in this regard limits the potential for a full assessment and accurate interpretation of data when studying breakdown injuries, as differences may reflect age, gender, size, or inter-animal variation. An understanding of normal and population variance is essential to fully utilize recent advancements in imaging and other technologies being utilized to investigate the effects of high speed exercise and race training on PSB structure and function.[8,9,10,11]

1.2 Medical diagnostic imaging

Radiographic imaging is commonly used in orthopedic diagnostics, including x-radiation imaging (x-ray, radiographs), computed tomography (CT), magnetic resonance imaging (MRI), and positron emission tomography (PET) scanning, in addition to diagnostic tools such as nuclear scintigraphy and perineural anesthesia for chronic fracture diagnosis.[6]

X-ray is a traditional diagnostic tool used for imaging skeletal tissues and has become popular in veterinary medicine due to affordability and portability of units.[12] Images are made by shooting x-ray waves from a source, through a region of the body towards an x-ray detector containing radiographic film.[13,14] Electromagnetic waves, which make up x-rays, were first observed by Michael Faraday in 1831.[13] In 1895, while using electromagnetic rays within a glass vacuum, Wilhelm Conrad Röntgen accidentally discovered the ability of these x-rays to image the skeleton.[13] The medical field quickly developed instruments specifically for their use, with the first full skeleton x-ray being taken in 1897 by William Morten.[13] X-rays are able to work because objects with high densities and higher atomic numbers (protons within the nucleus) will absorb more electromagnetic waves, while objects with lower densities will allow more x-rays to be transmitted to the surface of the detector.[14] This results in bone, which is denser than surrounding soft tissues and fluids and also has a higher atomic number due to high levels of Ca^{2+}, showing up with more contrast compared to other tissues.[14] This makes x-ray a good imaging tool for detecting fractures and arthritis as well as a diagnostic tool for other causes of lameness in horses.[12]

MRI is an imaging technique that is sensitive to soft tissue changes caused by inflammation or injury, including changes to the structure or fluid content.[12,15] Paul Lauterbur and Peter Mansfield are credited with publishing, though independently from each other, modern MRI technique in 1974.[16] However, there is a long history that lead to the development of MRI, also termed Nuclear Magnetic Resonance (NMR). This history reaches as far back as Jean Baptiste Joseph Fourier and Nikola Tesla, who developed the mathematics required to efficiently utilize MRI and discovered rotating magnetic fields, respectively.[16] Because MRI relies on magnetic fields and hydrogen ions within the body instead of radiation, there is no risk of radiation exposure and, thus, the technique is considered "safer" compared to imaging that requires the use of x-rays.[12,15] Orthopedic application of MRI includes the diagnosis of soft tissue injuries and pathology of articular cartilage and is frequently used in conjunction with other imaging techniques.[17,18,19] However, MRI requires a longer scan time and is more expensive than other scanning modalities.[12]

PET scanning is an imaging technique that relies on the injection of radioactive substrate into a patient to observe organ uptake of that radioactive material.[20] PET scanning developed in three phases. The first phase includes the discovery of positrons (or antielectrons) that carry positive charges within the electron cloud, originally proposed by Paul Dirac in 1929 and then confirmed by Carl Anderson in 1932, and development of the cyclotron by Ernest O. Lawrence (U.C. Berkley) between 1930 and 1936.[21] The second phase involved continued development of the cyclotron and image advancements, including single-photon tomography and CT imaging.[21] The final phase resulted in the development of the modern PET systems, with the prototype PET II built between 1972

and 1973 and the clinically applicable PET III being available by 1975 (Phelps, Hoffman, Mullani and Ter-Pogossian, Washington Univ.).[21] PET scanning is used largely in oncology, heart, or neuropsychiatric applications in humans, but it is becoming increasingly popular for orthopedic evaluation, often used in conjunction with CT.[12,20,22] However, more research is needed to understand the diagnostic capabilities of PET scanning when performing orthopedic evaluations in horses.

CT was the main imaging modality utilized in the investigations done for this thesis and will be discussed further going forward. Allan MacLeod Cormack, a theoretical physicist, and Godfrey Newbold Hounsfield, a medical researcher, are credited with inventing CT imaging, jointly winning the Nobel Prize for Physiology and Medicine in 1979.[13] Hounsfield patented his device in 1968 and his first clinically applicable instrument, the EMI Mark I, was operational by 1971.[13] The Hounsfield Unit (HU), a scale used to show radiodensity in CT images, is named after him. CT is commonly used in equine veterinary medicine for imaging the brain and head, specifically in neurologic horses.[23,24,25] There exists interest in utilizing CT as an imaging tool in musculoskeletal and orthopedic medicine due to superior diagnostic abilities created by highly detailed, cross-sectional images. CT typically provides improved image quality compared to other imaging methods, while providing a larger assessment region than MRI within the same time.[12]

Two major limitations of x-ray imaging include superimposing of soft tissue and bone and the limitation of "opacities," or x-ray absorption through materials, able to be viewed on the image (typically limited to air, fat, soft tissue, bone, and metal).[26] CT imaging is able to address both of these issues. First, the manner in which CT images are

saved and stored, called DICOM images, allow for them to be viewed in multiple planes, projected as three-dimensional structures, and removes the issue of superimposed tissues.[12,26] Second, CT instruments are more sensitive to x-ray absorption differences, allowing for more detailed imaging showing hundreds of different opacities from air to solid metals.[26] The image can be optimized for viewing a specific tissue type or anatomical site by changing the window width and window height, which modifies the opacities of certain tissues within image slices.[26]

The improved imaging ability of CT generally allows for better visualization and diagnostics within complex musculoskeletal structures, such as joints.[26,27] Continuing technological advances are addressing early limitations of CT, particularly the inability to scan live, standing horses in a reasonable timeframe.[12]

1.2.1 Clinical Computed Tomography

CT imaging used in diagnostic medicine is typically termed clinical CT (cCT). Individual slice thickness typically ranges from 0.5 mm to 6 mm, depending on application of the CT scan and the body region of interest.[28] Due to improved image quality (discussed in the previous section), cCT imaging is becoming ever more popular in equine diagnostic medicine. Tools exist to interpret cCT images at a structural level, including specialized DICOM viewers and programs that are able to measure Bone Mineral Density (BMD).

DICOM files can be viewed with DICOM viewer software. There are many different DICOM image viewers and packages, but the one used for this project was OsiriX MD DICOM Viewer (Pixemo SARL, Geneva, Switzerland).[29] The abilities of these viewers vary, though they will likely include tools to change window width and height (the

grayscale used to observe different tissue density), zooming, and orientation; region of interest (ROI) measurement tools such as area, length, and volume measurements; and projection tools such as plane re-sectioning and 3D renderings.

There also exist investigational software programs that can provide insight into the structural makeup of the bone. For this project, Mindways Software, Inc. QCT Pro™ Bone Investigation Toolkit (BIT) was used (Austin, TX).[30] Parameters provided by the QCT Pro™ BIT program are areal bone mineral density (aBMD), volumetric bone mineral density (vBMD), mass, area, and volume.

- aBMD (g/cm^2): calculated as bone mineral content of K_2HPO_4 (aqueous potassium phosphate) in grams divided by the projected bone area selected by the user defined RIO.[31,32,33]
- vBMD (g/cm^3): calculated as the bone mineral content of K_2HPO_4 in grams divided by the projected bone volume within the user defined RIO.[31,32,33]
- Mass (g): the K_2HPO_4 mass of the bone within the user defined ROI.[31,32]
- Area (cm^2): the projected area of the user defined ROI.[31]
- Volume (cm^3): the volume of the bone within the user defined ROI.[31]

BMD measurements of the medial PSB in post mortem warmblood foals (five and 11 months of age) have been reported to increase with age and have a clear response to training programs.[34]

1.2.2 Micro-Computed Tomography

For more detailed investigation into the internal structure of bone, micro-computed tomography (μCT) is necessary. While the slice thickness of cCT images is at the millimeter (10^{-3} meter) level, μCT is at the micron (10^{-6} meter) level, providing high resolution CT imagery at a resolution 1000 times greater than what is provided by most cCT instruments. This allows for high resolution assessments of the internal structure of materials such as bone, including the following parameters:

Total Volume (TV, mm^3, Figure 1.2.1), also known as tissue volume, is the total volume of all tissues within the sample; specifically, the total number of voxels in the sample, meaning that a larger sample will have a larger TV.[35] TV is more useful when compared to other parameters, such as bone volume. Horses suffering a PSB fracture breakdown have been reported to have a decreased TV when compared to control horses euthanized for reasons besides metacarpophalangeal (MCP), or fetlock, joint injury.[8]

Bone Volume (BV, mm^3, Figure 1.2.1) is the volume of the sample that is mineralized bone. Specifically, the number of voxels in the image classified as bone trabeculae.[35] BV is more useful when compared to other parameters, such a TV.

Bone Volume Fraction (BV/TV, %, Figure 1.2.2) is a proportion measurement calculated by dividing BV by TV. It indicates changes in bone micro volume, which occur prior to changes in BMD.[36] BV/TV has been reported to increase in horses suffering a PSB fracture breakdown when compared to control horses euthanized for reasons besides MCP joint injury and seen to decrease with age in humans.[8,37] There are two methods for determining BV/TV. The first divides the number of voxels classified as bone trabeculae

by the total number of voxels in the bone sample.[35] The second forms surface meshes over the bone (BV) and the total tested volume (TV) and then divides the two volumes.[38]

Connectivity Density (Conn.D, 1/mm^3, Figure 1.2.3) is a measurement of the degree of connection, a reflection of the trabecular network, within the bone and is calculated by dividing the connectivity estimate by TV.[39] The connectivity estimate is quantified by the Euler characteristic, a topographic invariant based on counting vertices, edges, and faces of an object such as a polyhedral.[39,40] Increased Conn.D contributes to bone strength, with decreasing values associated with human ageing.[37]

Trabecular Number (Tb.N), Trabecular Separation (Tb.Sp), and Trabecular Thickness (Tb.Th) are important characteristics that can help describe the internal architecture of bone (Figure 1.2.4). Tb.N (1/mm) is an estimate of the number of trabeculae within the sample. It is calculated as the inverse of the mean distance between the midlines of each trabeculae.[35] This parameter has been seen to decrease with age in horses and humans and is associated with an increased risk for vertebral fracture and decreases in BV/TV.[37,41]

The parameter abbreviated Tb.Th (mm) is the mean thickness of all trabeculae within the sample.[35,42] It has been reported to increase in horses suffering a PSB fracture in CMI events compared to control horses euthanized for reasons besides MCP joint injury.[8] While not seen to be effected by aging in horses, a decrease in Tb.Th is associated with the decrease in bone strength seen in aging men.[37,41] In contrast, trabecular separation (Tb.Sp, mm), also known as trabecular spacing, is the mean distance between the measured trabeculae.[35,42] Tb.Sp has been shown to increase with ageing in horses and humans, and greater Tb.Sp has also been associated with vertebral fracture in humans.[37,41] As these two

parameters are average values, there is variation in the exact Tb.Th and Tb.Sp across all trabeculae within a sample. Tb.Th and Tb.Sp are illustrated in Figure 1.2.5.

Degree of Anisotropy (DA) is a measure of how highly oriented the internal structure of the bone is.[43] It is calculated using the Mean Intercept Length method, where the length of the longest vector measurement is divided by the shortest vector measurement. A DA value =1 occurs when a structure is completely isotropic, meaning the internal structure is uniform in all directions.[42] Think of glass–if you have a glass cube, the cube would react to equal forces in different directions in the same way, no matter which direction the force was applied. A DA value >1 occurs when a structure is anisotropic, with larger values indicating increasing anisotropy.[42] This means that the internal structure of the material being measured is not uniform in all directions. Think of wood–there exists in all wood a grain which makes a force applied with the grain easier to split the wood compared to a force applied against the grain. Bone always has some level of anisotropy, often increased further by bone modeling in response to variations in biomedical forces caused by exercise and activity. Thoroughbred PSBs have been reported to be more isotropic in horses suffering from PSB fractures in association with CMI events when compared to control horses euthanized for reasons besides MCP joint injury.[8]

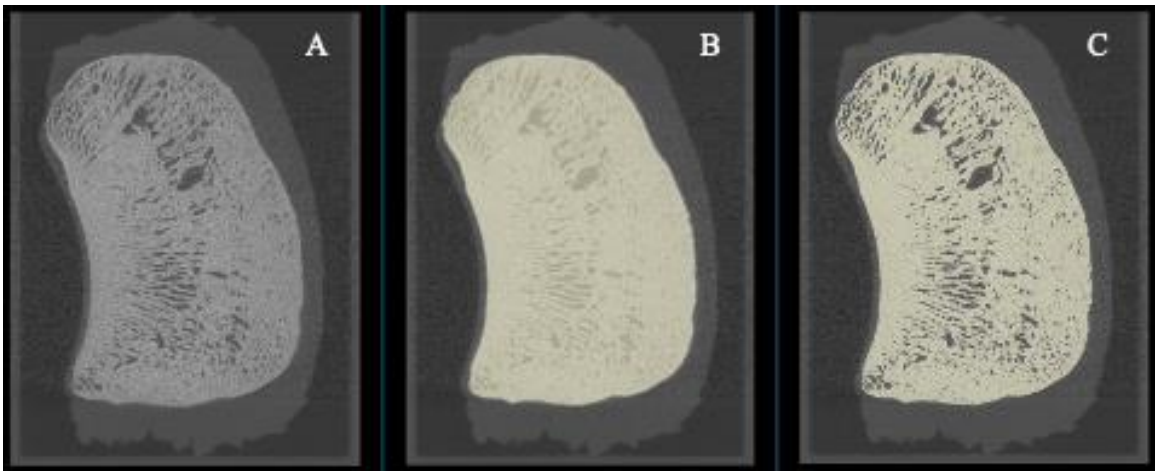

Figure 1.2.1: Micro-computed tomography (µCT) parameters Total Volume (TV) and Bone Volume (BV).
A. µCT image of an equine proximal sesamoid bone. B. TV, highlighted in the lighter cream color, is the total 3-demensional area (mm^3) of the sample being analyzed, both the mineralized bone matrix and the spaces between bone trabeculae. C. BV, highlighted in the lighter cream color, is the total 3-demensional area (mm^3) of the mineralized bone matrix. The dark spaces between bone trabeculae are not included in the BV value. Bone Volume Fraction, abbreviated BV/TV and expressed as a percentage, is a proportion measurement calculated by dividing BV by TV.

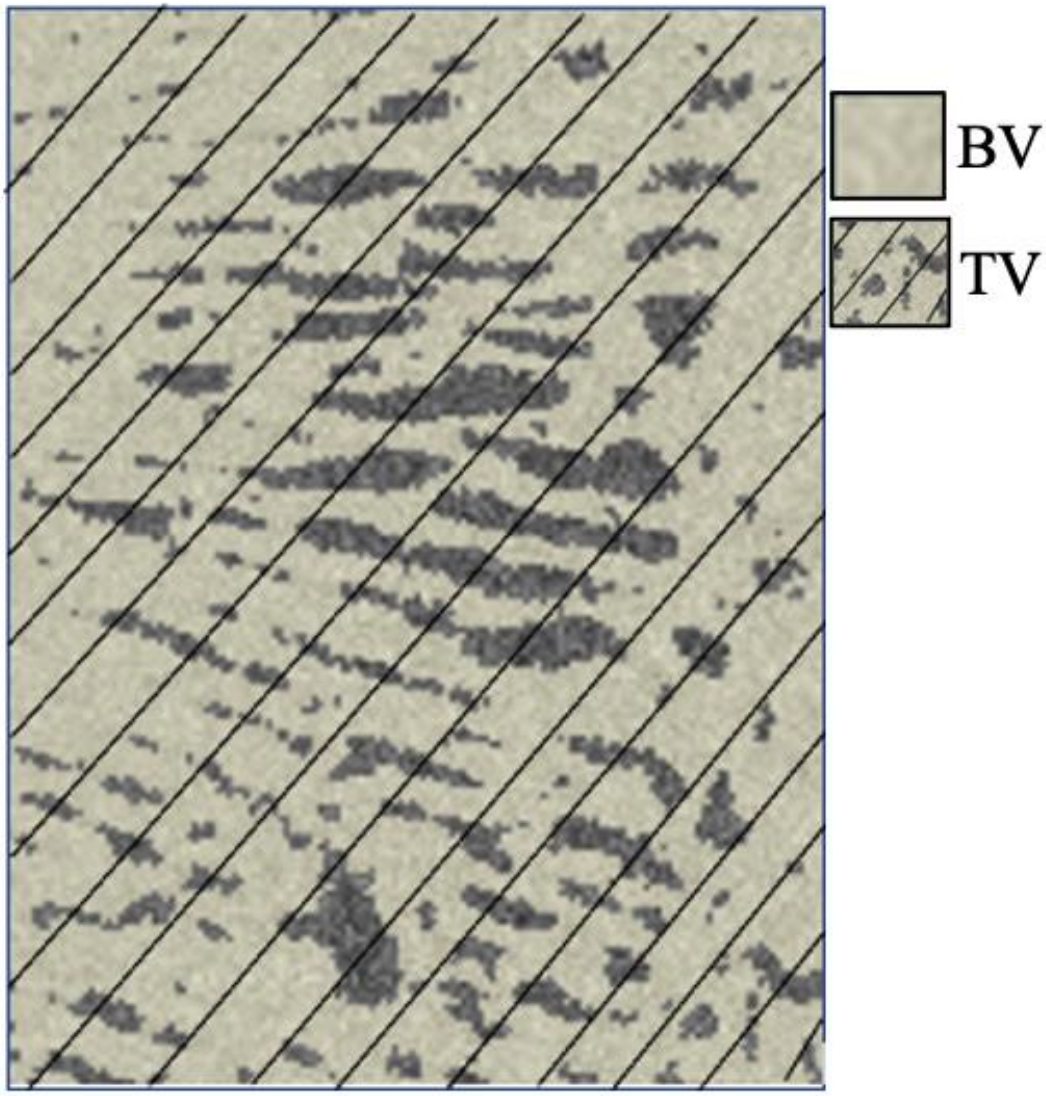

Figure 1.2.2: Visualization of Bone Volume Fraction (BV/ TV).

BV/TV is a micro-computed tomography (μCT) proportional measurement calculated by dividing Bone Volume (BV) by Total Volume (TV). Changes in BV/TV represent variations in bone micro volume prior to measurable differences in bone mineral density.

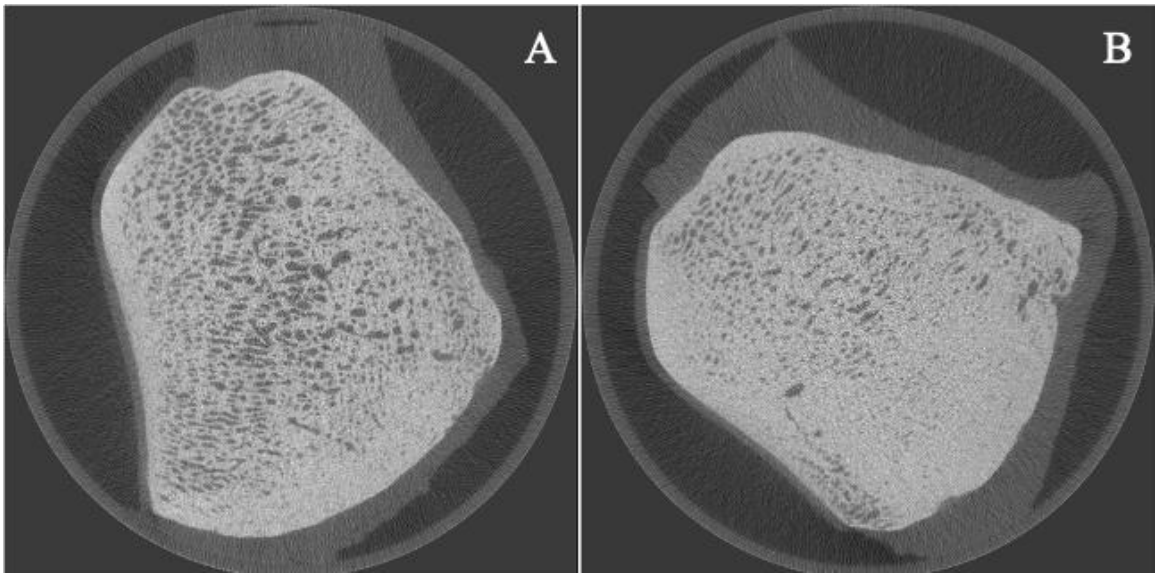

Figure 1.2.3: Depiction of Connectivity Density (Conn.D)

Conn.D is a micro-computed tomography (μCT) parameter the reflects the trabeculae structure within a bone. This is done by dividing the connectivity estimate, quantified by the Euler characteristic, divided by Total Volume (Conn.D units: $1/mm^3$). A. Increased Conn.D is linked to increased bone strength and increased trabecular number. B. Decreased Conn.D is seen in aging humans and is linked to decreasing trabecular number.

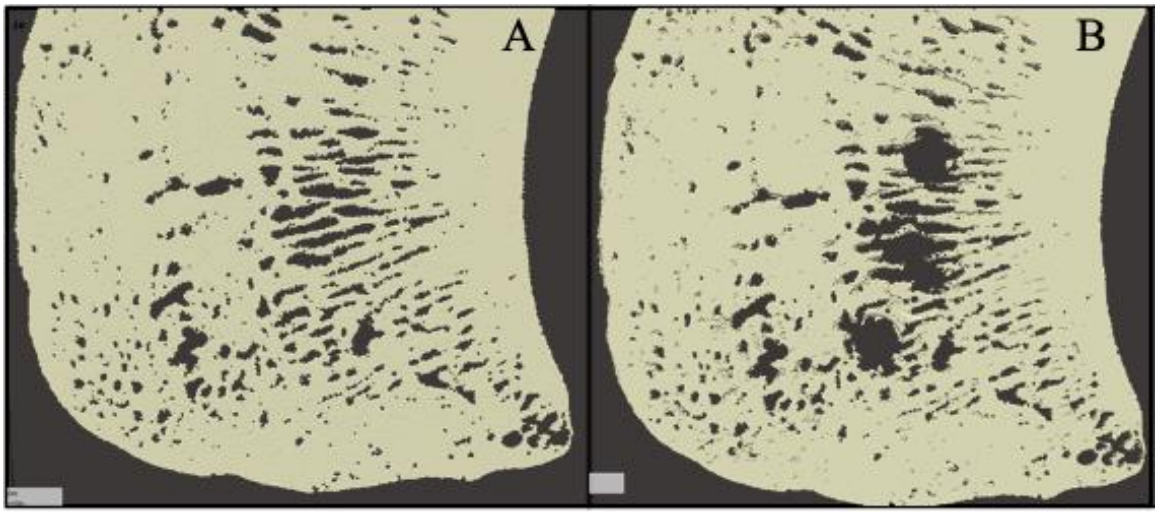

Figure 1.2.4: Micro-computed tomography (μCT) projection of Trabecular Number (Tb.N).

Tb.N is one of the three trabecular parameters measured by μCT bone morphometry evaluation. It is the estimated number of trabeculae within the bone and is an important characteristic that can help describe the internal architecture of bone. A. Normal Tb.N. B. Low Tb.N, indicated by large "holes" within the internal region of bone.

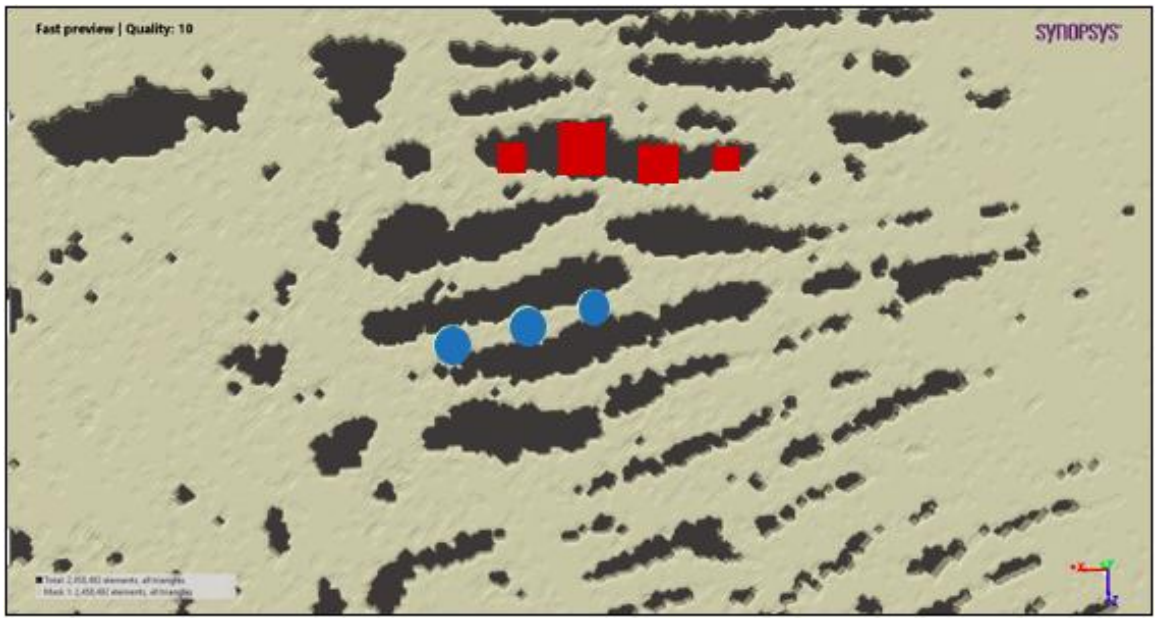

Figure 1.2.5: Micro-computed tomography (μCT) projection that depict Trabecular separation (Tb.Sp) and trabecular thickness (Tb.Th).
Tb.Sp, red squares, and Tb.Th, blue circles, are important characteristics that can help describe the internal architecture of bone. Tb.Sp (units: mm) is the mean distance between the measured trabeculae. Tb.Th (units: mm) is the mean thickness of all trabeculae within the sample.

1.3 Sesamoid Bones

Sesamoid bones are typically small, rounded bones that anatomically are found either connecting tendons or embedded within a tendon or ligament system. The PSBs are one of the three types of sesamoid bones found within the horse. Those three types are:

- Patella: a roughly oval bone found within the stifle joint of a horse; every horse has two, one within the stifle joint of each hind limb.
- PSBs: paired, triangular bones found within the palmar/plantar aspect of the metacarpo- and metatarso-phalangeal joints (MCP, MTP joints), also known as the fetlock joints; embedded in the suspensory apparatus and articulating with the distal condyles of the third metacarpal (MC3, cannon bone) and the proximal condyles of the first phalanx (P1); horses have two PSBs within each limb, one medial and one lateral, for a total of eight.
- Distal sesamoid (navicular) bones: shuttle-shaped bones found within the hoof dorsal to the deep flexor tendon and articulating with the second and third phalanx; every horse has four, one within each limb.

The PSBs are found embedded within the suspensory apparatus, with many layers of soft tissue preventing easy dissection or evaluation. From deep to superficial, the following describes the anatomy of the suspensory apparatus. The proximal aspect of the PSBs is the insertion sight for the branches of the interosseous muscle (IM, suspensory ligament), while the distal aspect serves as the proximal entheses of the distal sesamoidean ligaments (oblique and straight).[44] The intersesamoidean ligament connects the PSBs at the axial aspects of the bones.[44] The collateral sesamoidean ligaments originate from the

abaxial aspects of the sesamoids and insert at the proximal end of P1.[44] The deep digital flexor tendon (DDFT) and, overtop, the superficial digital flexor tendons (SDFT) run between the PSBs at their palmer surface, with the Manica Flexoria surrounding both tendons.[44] The palmar (or plantar in the case of hind limb) annular ligament covers the sesamoids on the palmar aspect of the fetlock joint, creating a sheath for the DDFT and SDFT.[44]

Dimensional size differences exist between medial and lateral PSBs. It has been previously reported in Thoroughbred horses that lateral PSBs are longer in length than medial PSBs, with no limb differences (right or left) seen.[4,45,46] There currently exists no consensus on PSB width. Anthenill et al. (2006) found medial PSBs of racehorses are wider than lateral PSBs in the LF but not in the RF.[4] When comparing limbs, the PSBs of the RF were seen to be wider than the PSBs of the LF.[4] Beccati et al. (2013) found similar medial to lateral PSB width asymmetry within their sample set only prior to the onset of training, with the medial PSB being wider in both forelimbs.[46] These findings have led to the general assumption that medial PSBs are typically shorter and broader, while lateral PSBs are typically longer and more narrow. However, Alrtib et al. (2013) saw no statistically significant relationship between medial and lateral PSB widths.[45] With their added measurement of depth, it was observed that lateral PSBs tended to be deeper than medial PSBs.[45] When measuring the other structures in the MCP joint, the medial condyle of the MC3 was found to be wider and deeper than lateral.[45]

1.3.1 Proximal Sesamoid Bone Biomechanics

Sesamoid bones in general have a function of decreasing wear and tear on the anatomical structures associated with them. This is achieved by decreasing friction between the anatomical structures during joint movement, absorbing and redistributing forces, and enhancing and protecting the power production of connected muscles. Functions of equine PSBs are specifically to provide stability to the suspensory apparatus and MCP joint and to prevent hyperextension of the MCP joint during the stance phase of locomotion.[47] This is a result of suspensory apparatus function, which is to store and release energy during the cycle of locomotion, decreasing the energy expenditure of the horse.[48,49]

During the stance phases of locomotion, the MCP joint transmits the greatest amount of contact force at each of the equine gaits compared to other joints within the forelimb.[49,50] Based on modeling, these forces originate solely from the biomechanics of the suspensory apparatus structures, most notably IM, SDFT, and DDFT, and they increase at faster gaits.[49,50,51] As the MCP joint hyperextends during the stance phase, the forces created by the suspensory apparatus cause the PSBs to become displaced, creating articulation between the condyles of MC3 and the PSB articular surface.[47] The result is two main sources generating the forces that move through the proximal sesamoid bone: the antiparallel forces of the attached ligaments and tendons of the suspensory apparatus and the contact force between the articular surfaces of the PSB and the MC3 (Figure 1.3.1).

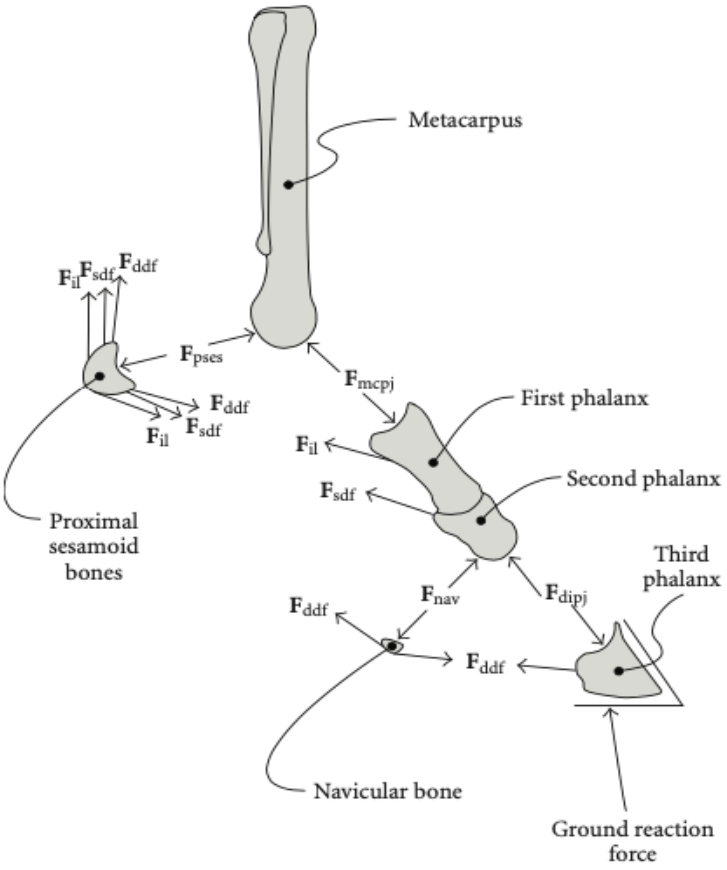

Figure 1.3.1: Forces within the distal forelimb.

During the stance phase, the metacarpophalangeal (MCP) joint transmits the greatest amount of contact force at all gaits. Due to the functionality of the suspensory apparatus, the proximal sesamoid bones (PSBs) experience two main forces: the antiparallel forces created by attached ligaments and the contact force created between the PSBs and the third metacarpal. Reprinted from "Influence of Muscle-Tendon Wrapping on Calculations of Joint Reaction Forces in the Equine Distal Forelimb," by J.S. Merritt, H.S.M. Davies, C. Burvill, and M.C. Pandy, 2008, *BioMed Research International(2008)*, 9 pages. Copyright (2008) by Hindawi.

1.4 Bone Development and Maturation

Most musculoskeletal tissues are derived from the mesoderm, with the exception of the craniofacial complex, which develops from ectomesenchyme and neural crest cells.[52] The axial skeleton is derived from the paraxial subdivision of the mesoderm, with vertebrae and their tendons forming from the sclerotome and skeletal muscles arising from the myotome.[52]

Limb bone development is a more complex process than the development of the axial skeleton. A limb bud first forms during early fetal development, arising from the proliferation of mesenchymal cells from the lateral subdivision of the mesoderm (bones and tendons), as well as from the myotome of the paraxial mesoderm (skeletal muscle).[52] The limb mesenchyme stimulates a signaling center to be established in the ectoderm, which releases fibroblast growth factors (FGF) to pattern the proximal to distal axis.[52] A zone of polarizing activities is also formed, expressing sonic hedgehog and patterns anterior-posterior patterning in the limb.[52] Eventually, the mesenchymal cells stop proliferating and start to condense in areas were future bones will form, though the exact signaling pathway is not fully understood at this time.[52] The interzone, a localized region of dense cells which later becomes the joint tissues, develops during mesenchymal condensation of the limb.[52]

1.4.1 Mechanisms of Bone Development

There are two mechanisms of bone formation which create the variety of bone shapes seen throughout the body. Intramembranous bone formation occurs when undifferentiated mesenchymal cells differentiate into osteoblasts that start laying down

bone matrix without an intermediate cartilage template stage.[52] This process is more straightforward than endochondral bone formation and occurs primarily in the bones of the skull and other flat bones.[52]

In contrast, endochondral bone formation is the process by which most mammalian bones, including long, short, and irregular bones, are formed and is a more complex process compared to intramembranous bone formation. Mesenchymal cell condensations differentiate into two different cell types, chondrocytes and perichondrial cells, signaled by Sox9 transcription factor.[52] Chondrocytes form the vascular-free inner portion of the condensation and perichondral cells generate the vascular-dense outer layer surrounding the chondrocytes.[52] Chondrocytes initially proliferate, though as the cartilage enlarges, the center chondrocytes cease proliferation and undergo hypertrophy (hypertrophic chondrocytes).[52]

Chondrocytes in flanking regions start to differentiate, forming the fetal growth plate.[52] Round chondrocytes make up the majority of cells in the head portion of the cartilage, exhibit a moderate rate of proliferation.[52] Periarticular chondrocytes are a group of round chondrocytes at the end of the cartilage that forms the joint surface.[52] Flat chondrocytes are formed from round chondrocytes located in the shaft near the hypertrophic chondrocytes that flatten.[52] They continue to proliferate, forming columnar chondrocytes.[52] They eventually change morphology again to become hypertrophic chondrocytes that no longer proliferate but instead progress through hypertrophy and cell swelling.[52] Chondrocyte hypertrophy, rather than cell proliferation, actually contributes most of the linear length to elongating the cartilage template during fetal bone growth.[52]

Perichondrial cells assume flat fibroblastic cell morphology, though their function is still an active area of investigation.[52] Chondrocytes and perichondrial cells communicate with each other through FGF and bone morphogenic factor (BMP) signaling.[52] Some perichondrial cells become osteoblasts that populate the cortical and trabecular bone later on.[52] There are three distinct functional areas of the perichondrium along the cartilage:

- Periround layer at the head.[52] Distinctly ambiguous with the chondrocytes until joint and articular development are fully complete postnatally.[52] Some express Sox9 and are involved in the development of tendon insertion sights and bony eminesses.[52]
- Periflat layer at the base.[52] Form a distinct notch called the perichondrial groove of Ranvier that may work as a signaling center.[52]
- Perihypertrophic layer at the shaft.[52]

Some cells become osteoblasts while others become periosteum cells, depending on underlining hypertrophic chondrocytes and cell singaling.[52]

The primary ossification center is established by a network of trabecular bone and blood vessels, which continues to enlarge along with the marrow cavity as the growth plate continues to grow further out (mechanism not clear).[52] Secondary ossification centers can form within a long bone at the epiphyseal cartilage at both ends of the bone.[52] Similar to the primary ossification center in that it is composed of a highly vascular marrow space enriched with trabecular bone; however, it is surrounded by chondrocytes of the fetal growth plate and articular surface instead of the perichondrium and bone collar.[52] The postnatal growth plate is a disk formed between the primary and secondary centers of

ossification and is composed of columns of chondroyctes.[52] It is similar to the fetal growth plate, with the biggest difference being a slower rate of proliferation of chondrocytes resulting in slower bone growth.[52]

1.4.2 Sesamoid Bone Development

As previously mentioned, sesamoids are small, rounded bones embedded in a tendon or ligament system which usually make up part of a joint system. Because of their diversity in size and shape, sesamoid bones do not fit within normal bone classification, though they are occasionally classified as short or irregular bones. The standard model for sesamoid development was proposed as early as 1904, wherein the sesamoid bone develops within a tendon separate from the long bones of a joint in response to embryonic movement.[53,54,55]

The patella is the largest and most recognizable sesamoid bone in the human body, a component of the patellofemoral, or knee, joint.[56] This has resulted in a great amount of research investigating the development of these large sesamoid bones. Cell condensation for a cartilaginous patella has been reported as early as 7.5 weeks gestation in human fetuses.[57] This aggregation of cells develops within the interzone layers of the joint, forming a cartilaginous structure at the distal aspect of the femur by week nine of gestation.[57,58,59,60] Data presented by Anderson (1961) suggested that the cartilaginous patella may form first behind the extensor tendon, followed by invasion of the tendon later in development.[60] This is somewhat in contrast to the traditional model of sesamoid bone development.

More recently, an alternate model of sesamoid development has been proposed suggesting sesamoid bones originate from the long bones of a joint.[61,62] In this model, shown in mice, it is proposed that the sesamoids, including the patella, lateral flabella, and digit sesamoids, originate from long bones in a similar Sox9/Scx signaling process as bone superstructures of the long bone that then detach through a cell signaling process.[61,62] While the exact machination or process of sesamoid bone development may be disputed, there is clear evidence suggesting both mechanical forces and genetics contribute to their formation.[60,63,64]

1.4.3 Sesamoid Bone Maturation

Sesamoid bone maturation is better understood in humans, with the ossification timeline being well established in children. For the patella, primary ossification commences at four to six years of age in humans, initially with multiple small ossification centers that converge to form one primary ossification center.[58,65] This ossification typically lasts into the early teen years, with ossification extending out towards the margins irregularly until fully calcified.[58,65]

While incidence of MCP and MTP sesamoids varies within humans, the majority of the population has a minimum of two MCP sesamoids at the thumb, and two MTP sesamoids at the hallux (big toe).[55,66,67] Ossification of these sesamoids commences around nine years of age from one or more ossification centers.[55,66,67] While it was initially reported that the sesamoid bones of the MTP joints are fully ossified at around age 10, it was reported by Sun et al. (2021) that complete ossification occurs much later in life (age 26 in females and age 29 in males).[55,66,67]

The majority of experimental biology investigating sesamoid bone development and maturation has been done in humans and model organisms such as mice. Size, expense, and the long gestation interval has limited the use of horses in such studies. This has resulted in little reported information about the development and maturation of equine sesamoid bones, including the PSBs. It has been noted that proximal sesamoid bone ossification begins between 290 and 330 days gestation, with complete ossification occurring around three to four months post parturition.[68,69] Though full ossification is reported to be complete by four months post parturition, PSBs can increase in size until 18 months of age.[68] While little is known about the development of the cartilaginous sesamoid bones prior to the start of ossification, there is clear evidence from work in our laboratory of cell aggregation forming at the sight of PSB development as early as day 46 in gestation (Figure 1.4.1).

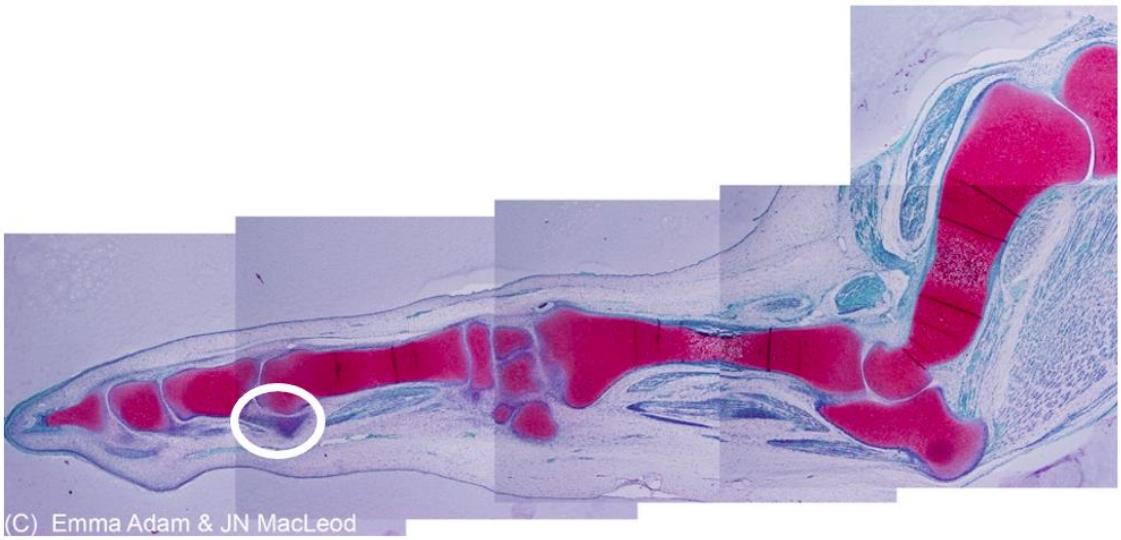

Figure 1.4.1: Safranin-O staining on 46 day gestation fetus.
Safranin-O staining performed on the forelimb of a 46 day gestation fetus depicting cell aggregation at the future sight of the PSBs (white circle). This indicates that PSB development occurs early in the gestational timeline, highlighting the knowledge gap of fetal sesamoid development prior to ossification. Image courtesy of Adam, Lowney & MacLeod – unpublished.

1.5 Knowledge Gap

As previously mentioned, there exists limited published data on the normal maturation, structural anatomy, and population variation of PSBs. This limits the ability to interpret data investigating the cause of PSB fracture and CMI injuries in racehorses, along with any other pathologies. Currently, a great amount of research is being done to understand the cause and mechanism of PSB fracture and suspensory apparatus failure in racehorses.[8,9,10,11] However, the ability to interpret these findings is limited by the lack of *normal* population values for measured parameters, as well as inter-animal variation. The objective of this study is to provide normalized baseline knowledge of PSBs in healthy horses, including the maturation timeline and a preliminary assessment of variation between individuals. Data that helps to address this knowledge gap will substantially facilitate the analysis and interpretation of future studies investigating CMI events involving PSB fractures.

1.5.1 Addressing the Knowledge Gap

There is little understanding of the normal postnatal maturation process for equine PSBs. The broad objective of this project is to increase the knowledge and understanding of *normal* maturation, structural anatomy, and population variation within normal Thoroughbred horses. The more specific question being investigated is whether anatomical

and structural parameters of postnatal equine PSB maturation will have gender-dependent differences and correlate with MC3 medial-lateral width at the MCP joint. This will be done through three specific aims.

Specific Aim 1 will determine if a correlation exists between the medial to lateral width of the MC3 at the MCP joint and anatomical or structural parameters of PSB maturation in Thoroughbreds. Forelimb cCT scans will be collected on horses aged two to six years old from a collaborating equine hospital. Dimensions of the PSB and the MC3 will be determined using OsiriX MD DICOM Viewer. Statistical analyses will be done to determine if there is a correlation between PSB size and the width of the MC3 medial-lateral width. Anatomical dimensions will also be compared to µCT BME and cCT BMD structural parameters to determine if there are any correlations.

Specific Aim 2 will determine if there are differences in anatomical or structural parameters between the medial and lateral PSBs in the front limbs of Thoroughbreds. PSB samples will be analyzed across the entire timeline, birth (zero days post parturition) to six years of age, utilizing µCT Bone Morphometry Evaluation (BME) with the following structural parameters assessed: TV, BV, BV/TV, Conn.D, Tb.Th, Tb.N, Tb.Sp, and DA. Clinical CT scans will be collected on horses aged two to six years old from a collaborating equine hospital. The DICOM files will be uploaded to QCT Pro™ BIT and examined to provide BMD measurements. The medial and lateral PSBs will be compared to determine any significant differences in parameters. The potential for gender- or age-dependent differences will be analyzed using comparative statistics.

Specific Aim 3 will compare changes of anatomical and structural parameters during PSB maturation in male and female Thoroughbreds as a function of postnatal age

from birth (zero days post parturition) to six years of age. Maturation of PSB samples will be analyzed across the entire timeline utilizing µCT Bone Morphometry Evaluation (BME) with the following structural parameters assessed: TV, BV, BV/TV, Conn.D, Tb.Th, Tb.N, Tb.Sp, and DA. Clinical CT scans will be collected on horses aged two to six years old from a collaborating equine hospital. The DICOM files will be uploaded to QCT Pro™ BIT and examined to provide BMD measurements. A point of maturation will be determined for the proximal sesamoid bones for each µCT BME parameter.

CHAPTER 2. PROXIMAL SESAMOID MATURATION IN NORMAL POPULATIONS

2.1 Introduction

Musculoskeletal injuries and lameness are a major cause of early termination of racing careers in Thoroughbred racehorses, including catastrophic musculoskeletal injuries (CMI) resulting in horse death.[1,2] In 2020, it was reported that there were 1.41 racing fatalities reported for every 1000 starts (includes musculoskeletal injuries, non-musculoskeletal injuries, and sudden deaths).[3] Of those fatal outcomes associated with CMI, proximal sesamoid bone (PSB) fracture is present in 40% to 50% of cases.[5,4] Most common are biaxial fractures (present in 80% of case), where both the medial and lateral PSB are fractured, localized to midbody and basilar regions of the PSBs.[4] PSB fractures are also common fatigue injuries in young foals under two months of age, suffered during periods of strenuous exercise, often when running after their dam in pasture.[7]

Due to these epidemiological data, there is substantial interest in better understanding the cause and mechanism of PSB fracture and suspensory apparatus failure.[8,9,10,11] One challenge is that there exists little information on *normal* PSB development and maturation, and on expected levels of inter-animal variation in the population. This leaves a critical knowledge gap of how variables such as age, size, and gender effect PSB structural anatomy. The goal of this study is to provide *normalized* baseline knowledge of PSBs in healthy horses, including a postnatal maturation timeline and a preliminary assessment of variation between individuals within the Thoroughbred breed.

Three experiments were conducted:

Experiment 1 investigates normal PSB anatomy by measuring the dimensions of the MC3 and PSBs of the forelimbs, taken from cCT DICOM images from horses aged two to six years old. The width of the MC3 at the MCP joint will be compared to anatomical dimension of the PSBs to determine if there are any correlations. Anatomical dimensions will also be compared to µCT BME and cCT BMD structural parameters to determine if there are any correlations.

Experiment 2 investigates the normal PSB internal structural anatomy and population variation through the use of µCT BME in horses aged from birth (zero days post parturition) to six years old and cCT BMD evaluation in horses aged two to six years old. Anatomical and structural parameters are compared between the medial and lateral PSBs in the front limbs of Thoroughbreds to determine if differences exist. The potential for gender- or age-dependent differences are analyzed using comparative statistics.

Experiment 3 investigates the PSB maturation timeline and internal structural anatomy through the use of µCT BME in horses from birth (zero days post parturition) to six years old and cCT BMD measurements in horses aged two to six years old. The issue assessed is how PSB structural parameters change during the skeletal growth and maturation phase of young Thoroughbreds, and to determine if there is an age at which the parameters stabilize and age-dependent changes are no longer observed .

The board objective of this project is to increase the knowledge and understanding of *normal* maturation, structural anatomy, and population variation within normal Thoroughbred horses.

2.2 Materials and Methods

2.2.1 Experimental Sample Set

A total of 108 PSBs from 36 Thoroughbred horses were analyzed in this study (Table 2.2.1). The gender distribution was 17 females, 14 intact males, and five neutered males. The age distribution was zero (day of foaling) to 2219 days (Figure 2.2.1). The individual samples (horses) used for cCT, μCT, or both are listed in Table 2.2.1, with selection based on achieving approximately even distribution across the experimentally targeted age ranges. Both unraced and actively training/competing horses were included in the sample set. No horses that had suffered a CMI were included; however, minor skeletal changes consistent with the demographic of young Thoroughbred racehorses were not considered a basis of exclusion. As such, all of the horses in the study were assessed as "population normal" with regard to PSB and fetlock joint gross and cCT imaging parameters by collaborating veterinarians (Drs. Garrett, Janes, and Kennedy). A list of any necropsy or cCT imaging findings for the horses used in this study can be found in Appendix 2.

Table 2.2.1: Sample set demographics

Table containing gender, age (year, month, and day), CT category participation, number of sesamoids scanned, and racing information for all 36 Thoroughbred horses.

Sample	Gender	Age (year)	Age (months)	Age (days)	µCT scan	cCT scan	Number of Sesamoids Scanned	High Speed Work	Racing Starts
1	M	0	0	0	Y	N	2	N	NA
2	F	0	0	0	Y	N	2	N	NA
3	F	0	0	3	Y	N	2	N	NA
4	M	0	0	4	Y	N	2	N	NA
5	F	0	1	43	Y	N	2	N	NA
6	F	0	4	120	Y	N	2	N	NA
7	M	0	5	145	Y	N	2	N	NA
8	M	0	6	170	Y	N	2	N	NA
9	F	1	12	365	Y	N	2	N	NA
10	M	1	17	517	Y	N	2	N	NA
11	M	2	20	616	N	Y	4	Y	0
12	F	2	21	645	Y	N	2	Y	0
13	F	2	24	726	N	Y	4	Y	0
14	F	2	24	742	N	Y	4	Y	0
15	F	2	25	755	Y	Y	4	N	NA
16	M	2	27	812	N	Y	4	Y	0
17	NM	2	27	813	Y	Y	4	Y	0
18	M	2	29	888	Y	N	2	Y	2
19	M	2	32	961	N	Y	4	Y	3
20	F	2	35	1050	Y	Y	4	Y	0
21	F	3	37	1135	N	Y	4	Y	5
22	M	3	39	1180	N	Y	4	Y	3
23	F	3	39	1186	Y	Y	4	Y	5
24	NM	3	43	1301	N	Y	4	Y	0
25	F	3	43	1306	N	Y	4	Y	12
26	M	3	45	1355	Y	N	2	Y	4
27	NM	3	47	1418	Y	Y	4	Y	7
28	F	4	48	1456	Y	N	2	N	NA
29	M	4	49	1499	N	Y	4	Y	2
30	F	5	60	1825	Y	N	2	N	NA
31	M	5	60	1825	Y	N	2	N	NA
32	M	5	64	1960	Y	N	2	Y	17
33	NM	5	65	1984	N	Y	4	Y	23
34	NM	5	66	2018	Y	N	2	Y	13
35	F	6	71	2172	Y	Y	4	Y	55
36	F	6	73	2219	N	Y	4	Y	39

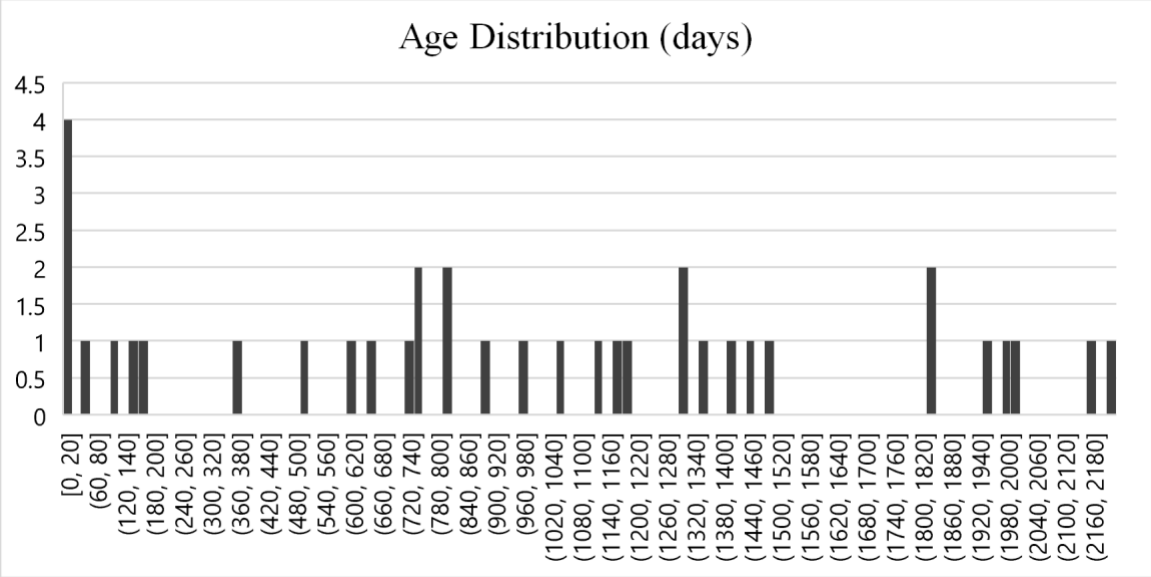

Figure 2.2.1: Age distribution

The age distribution of the 36 Thoroughbred horses in the sample set from birth to six years of age. A priority for sample selection was to achieve an even distribution across the entirety of the age range, allowing for good representation of proximal sesamoid bone maturation until six years of age.

2.2.2 Clinical Computed Tomography

Specimens were obtained postmortem from the University of Kentucky Veterinary Diagnostic Laboratory (VDL). Left front (LF) and right front (RF) limbs from 18 horses were amputated immediately above the carpus within 48 hours of euthanasia or death and stored in a 40ºF cooler. The limbs are transferred to a local equine hospital for cCT evaluation within five days of amputation and prior to PSB dissection. A NL4000 BodyTom Elite CT scanner (software version 1.08.10) was used, producing focused axial MCP scans of both limbs from each horse at 120 kV energy level (Neurologica Corporation, Danvers, MA).

The DICOM images for each limb were then uploaded to OsiriX DICOM Viewer (software version 11.0.1, Pixemo, Bernex, Switzerland). The cCT images were analyzed for dimensional measurements at specific anatomical sites as listed below and illustrated in Figure 2.2.2 using measurement tools in OsiriX utilizing the MPS 3D viewer.

- 3MC width taken 5 mm from the articular surface of the condyles, shown in purple in the axial plane.
- PSB width taken at the widest total point across both sesamoids parallel to 3MC width, shown in mustard in the axial plane.
- PSB depth at both the articular bulge and articular sulcus of 3MC perpendicular to the width line, shown in teal and pink, respectively, in the axial plane.
- PSB length at tallest point, shown in green in the sagittal plane.
- PSB straight and curved length of the articular surface, shown in orange and red, respectively, in the sagittal plane.

DICOM files for each limb were decompressed by OsiriX and exported to the desktop for upload into the Mindways Software QCT Pro™ software (version 6.1.90, Austin, TX). Once uploaded utilizing the "AWCDreader.ext," files were run through the Mindways Software QCT Pro™ Bone Investigation Toolkit (BIT), isolating each PSB while controlling high threshold at 300 mg/cc. PSBs were rotated to square the articular surface to the vertical plane facing right (axial view), square the basilar surface to the horizontal plane (sagittal view), and square the articular surface to the horizontal plane (coronal view), shown in Figure 2.2.2. A "User Defined" region of interest (ROI) was then

fit around the 3D projection of the PSB (Figure 2.2.3) and a report generated. The following parameters were recorded: areal bone mineral density (aBMD, g/cm^2), volumetric bone mineral density (vBMD, g/cm^3), Mass (g), Area (cm^2), and Volume (cm^3).

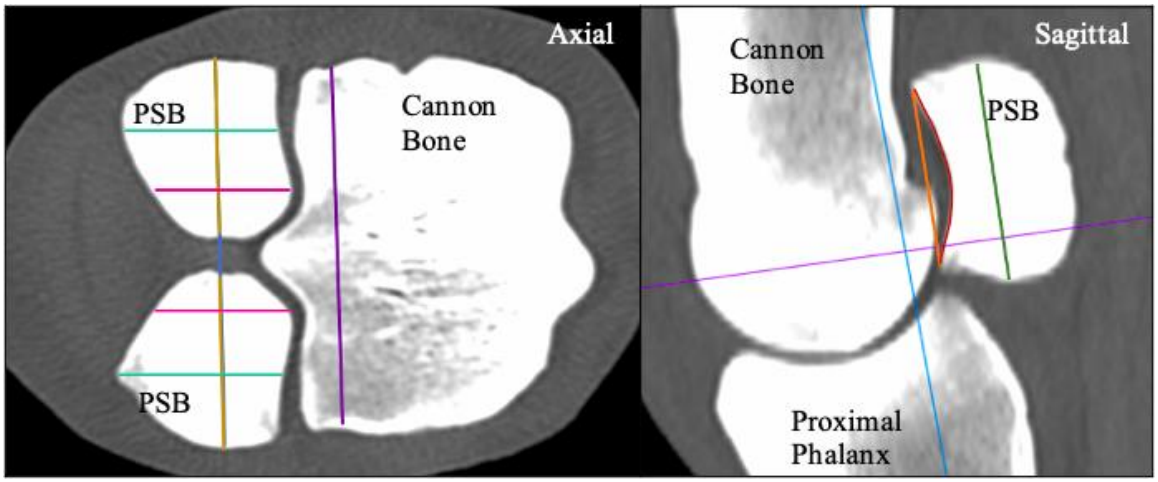

Figure 2.2.2: Dimensional measurements

Clinical computed tomography scans were uploaded into the OsiriX DICOM Viewer to determine dimensions of the proximal sesamoid bones (PSB) and third metacarple (MC3). Dimensions were taken in the Axial and Sagittal planes, using the MPS 3D viewer to prevent oblique angles through the limb that would distort the measurement. The following emasurements were taken: MC3 width (axial view, purple); PSB width (axial view, mustard); PSB depth at the MC3 articular bulge (axial view, teal); PSB depth at the MC3 articular sulcus (axial view, pink); PSB maximum length (sagittal view, green); PSB straight articular surface length (sagittal view, orange); PSB curved articular surface length (sagittal view, red).

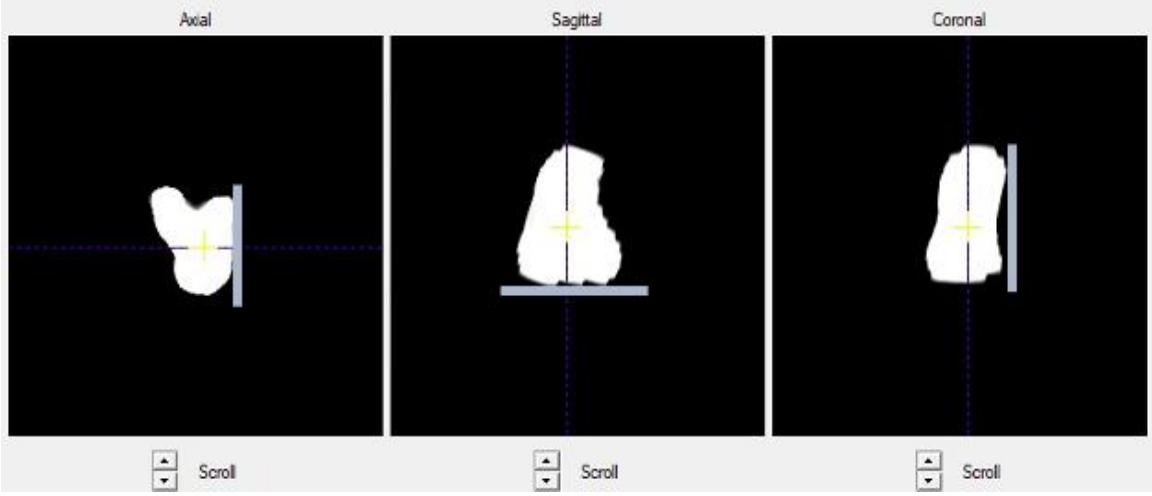

Figure 2.2.3: Proximal sesamoid bone (PSB) alignment in QCT Pro BIT program
Depiction of the required alignment for PSBs in the Mindways Software QCT Pro protocol. Consistent alignment was required to reduce user variability in area and volume measurements derived by the software to measure bone mineral density (BMD). The PSBs were rotated to square the articular surface to the vertical plane facing right (axial view), square the basilar surface to the horizontal plane (sagittal view), and square the articular surface to the horizontal plane (coronal view).

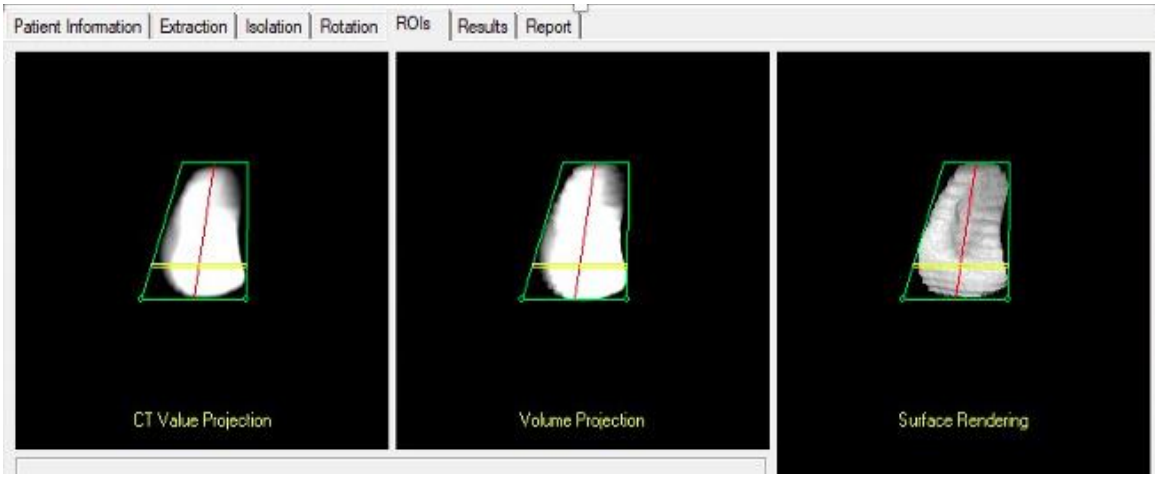

Figure 2.2.4: Shaping the Region of Interest (ROI)
Shaping the ROI around the PSB projections in the Mindways Software QCT Pro software software determined the area, volume, and mass measurements that were then used to calculate the bone mineral density (BMD). The RIO could be shaped into any quadrilateral shape to best fit around the PSB.

2.2.3 Micro-Computed Tomography

Specimens were obtained postmortem from the University of Kentucky VDL. The PSBs were dissected from the suspensory apparatus within 48 hours of euthanasia or death in one of two methods. For horses aged under 18 months, all eight PSBs of all four limbs were collected one to four days post necropsy examination. The LF and left hind (LH) PSBs were stored in 10% phosphate buffered formalin at room temperature and the RF and right hind (RH) PSBs were stored in lactated ringers solution (LRS) and frozen post collection. For horses aged over 18 months, limbs were amputated immediately above the carpus within 48 hours of euthanasia or death and stored in a 40ºF cooler. The four PSBs of the forelimbs were dissected from the limb within two to three days post limb amputation, frozen in LRS post collection, and then thawed and stored in 10% phosphate buffered formalin at room temperature. For samples aged over 18 months collected Spring 2020 and later, all four forelimb sesamoids were directly stored in 10% phosphate buffered formalin at room temperature without freezing. Medial and Lateral PSBs from the forelimbs of all samples were then separated prior to µCT scanning.

All 44 PSBs from 22 horses were scanned with a SCANCO Medical µCT 40 instrument (software version 6.1) utilizing the x-Ray scan setting with energy and intensity setting of 70kVp, 114 µAmps, and 8 W (SCANCO Medical, Wangen-Brüttisellen, Switzerland). Scans were then contoured and run through the Bone Morphometry Examination (BME) with settings of Gauss sigma 1.6, Gauss support 3, lower threshold 154, and upper threshold 1000. A lower threshold between 120 and 134 was used for samples that were aged from birth to 517 days, as each bone needed to be evaluated individually for optimal representation of bone volume due to variable levels of ossification

and growth. Output data were received for the following parameters: Total Volume (TV), Bone Volume (BV), Bone Volume Fraction (BV/TV), Connectivity Density (Conn.D), Trabecular Number (Tb.N), Trabecular Thickness (Tb.Th), Trabecular Separation (Tb.Sp), and Degree of Anisotropy (DA).

2.2.4 Statistical analysis

Analyses were run utilizing R (software version R 4.0.2) (R Core Team 2029==20) via RStudio IDE (RStudio 2018, Boston, MA). Each response variable was plotted against each predictor variable to determine if a relationship existed. Variables are listed in Table 2.2.2. A Pearson correlation was calculated between each pair of response variables, with correlations being considered strong at > 0.7. A linear mixed model was fit between each response variable and all the predictor variables, and partial F-tests determined predictor variables effect on response variables. Significance was determined by α=0.05. If gender had a significant effect, the Tukey procedure was used to test differences between groups (female, intact male, and neutered male).

Finally, nonlinear regression was used to fit an asymptotic exponential function to the relationships existing between age and BME response parameters using:

$$y = c + (y_0 - c)e^{-rx}$$

where c is the horizontal asymptote representing the average maximum morphometric measurement value at maturity, r is a rate parameter, y_0 is the y-intercept of the function, and x is age. To determine the point at which a plateau was reached with relative stability and the absence of continued age-dependent changes (if present), the following equation was used:

$$m = y_0 + p(c - y_0)$$

where p is the percentage of the difference between the average asymptotic value and the average initial value, set at 90%, and m is the measurement value that had been deemed to represent stability. Combining and solving for age x:

$$-\frac{1}{r} ln \frac{m - c}{(y_0 - c)} = x$$

The age in days at stability was x and was represented by a natural logarithmic function.

Table 2.2.2: Variables
All variables listed by type and the CT analysis method which produce them. Predictor variables include age, weight, gender (female, intact male, or neutered male), leg (left vs right front), and bone (medial vs lateral). Response variables included bone morphometry output variables coming from micro-computed tomography (μCT) analysis, bone mineral density measured clinical computed tomography (cCT), and dimensional measurements, also from cCT.

Variable Type	Variable	CT analysis
Predictor	Age	
	Weight	
	Gender	
	Leg (LF vs RF)	
	Bone (medial vs lateral)	
Response	TV	Bone Morphometry (μCT)
	BV	
	BV/TV	
	Conn.D	
	Tb.N	
	Tb.Th	
	Tb.Sp	
	DA	
	Volume	Bone Mineral Density (cCT)
	vBMD	
	Straight articular surface length	Dimensions (cCT)
	Depth articular bulge	
	Depth articular sulcus	
	Length	
	Width	
	MC3 Width	

2.3 Results

A correlation heat map was generated with all measured dimensional and structural parameters (Figure 2.3.1).

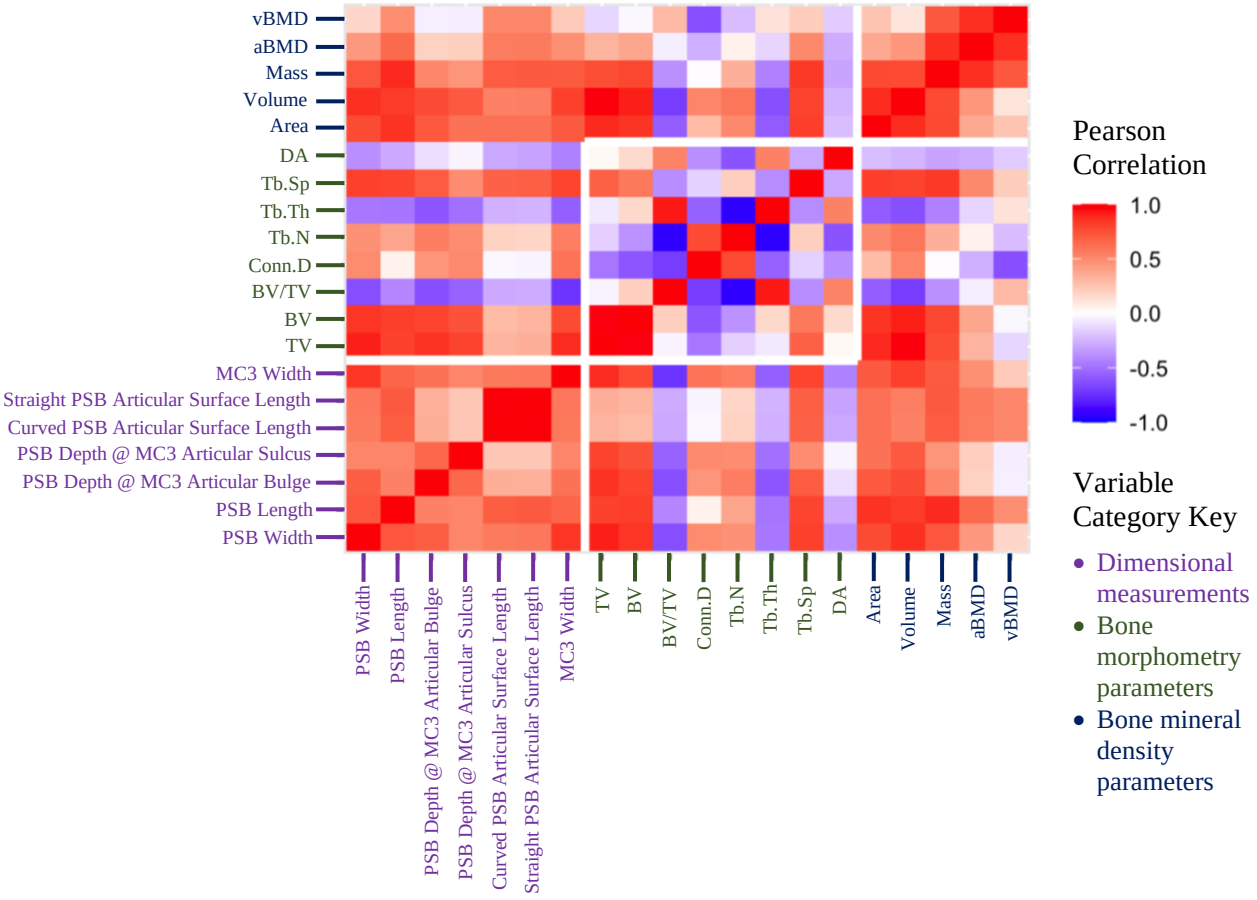

Figure 2.3.1: Heat map

A heat map depicting a Pearson's correlation for each pair of response variables. The map groups each type of response variable, bone morphometry measurements (green), bone mineral density measurements (blue), and dimensional measurements (purple). There were strong correlations with most dimensional measurements and volume measurements. Third metacarpal width had a strong positive correlation with proximal sesamoid bone width. Bone Volume Fraction (BV/TV) exhibited negative correlations with dimensional measurements and a strong negative correlation with Trabecular Number (Tb.N), but a strong positive correlation with Trabecular Thickness (Tb.Th). Tb.N displayed a strong negative correlation to Tb.Th. There also appeared to exist strong positive correlations between Trabecular Separation and dimensional measurements.

2.3.1 Experiment 1: Proximal Sesamoid Bone Dimensional Measurements

Linear mixed model results are provided in Table 2.3.1. Weight was a significant predictor for all dimensional measurements (p-value < 0.05), exhibiting a positive relationship in all cases. When comparing medial PSBs to lateral PSBs, the lateral bones were longer while the medial bones were deeper at the articular bulge for the medial bone than the lateral bone (p-value < 0.05, Figure 2.3.2). No dimensional measurements were different between LF and RF limbs ($p > 0.05$).

Strong correlations were observed between dimensional measurements and structural parameters (Table 2.3.2). Most notable were the correlations between MC3 width and PSB width (Pearson's coefficient of 0.8439014) and PSB length and PSB width (Pearson's coefficient of 0.7202423). There also existed notable correlations between dimensional measurements and structural parameters, including: MC3 width and Tb.Sp (Pearson's coefficient of 0.7916119), MC3 width and BV/TV (Pearson's coefficient of -0.7360496); PSB width and Tb.Sp (Pearson's coefficient of 0.8084853); and PSB length and Tb.Sp (Pearson's coefficient of 0.7938988). Strong correlations between parameters of volume and dimensional measurements were observed.

Table 2.3.1: Linear mixed model analysis of dimensional measurements

A linear mixed model was used to compare predictor variables to dimensional response variables. Weight was a positive predictor for all dimensional measurements ($p < 0.05$). Proximal sesamoid bone (PSB) length was greater in lateral PSBs ($p < 0.05$). PSB depth at the articular bulge of the third metacarpal was greater in medial PSBs $p < 0.05$).

Dimension	Comparison	P-value
3rd metacarpal width	Age	0.2508790
	Weight–Positive relationship	0.0315202*
	Sex	0.7981238
	Leg	0.3633446
PSB width	Age	0.1573528
	Weight–Positive relationship	0.0011501*
	Sex	0.8145239
	Leg	0.2729746
	Bone	0.0579438
PSB length	Age	0.0915171
	Weight–Positive relationship	0.0098451*
	Sex	0.9357410
	Leg	0.8162005
	Bone–Lateral PSB > Medial PSB	0.0000053*
PSB straight articular surface length	Age	0.0805637
	Weight–Positive relationship	0.0409933*
	Sex	0.4709754
	Leg	0.8967834
	Bone	0.9125914
PSB depth @ articular sulcus	Age	0.7009641
	Weight–Positive relationship	0.0381436*
	Sex	0.9239504
	Leg	0.1850623
	Bone	0.1633731
PSB depth @ articular bulge	Age	0.2521431
	Weight–Positive relationship	0.0063677*
	Sex	0.7533658
	Leg	0.8523694
	Bone–Medial PSB > Lateral PSB	0.0058678*

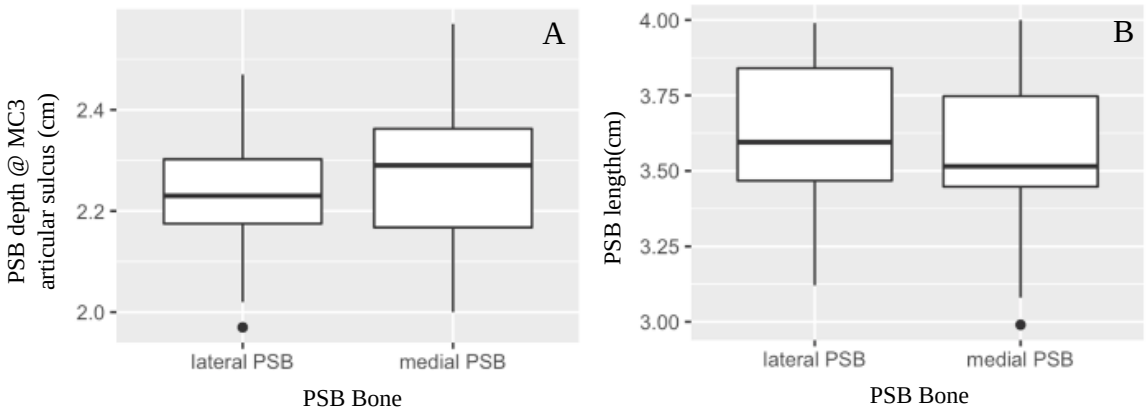

Figure 2.3.2: Box plots comparing significant medial-lateral dimensional differences A. Medial proximal sesamoid bone (PSB) depth was greater than lateral when measured at the articular bulge of the third metacarpal (MC3). B. Lateral PSB length was greater than medial.

Table 2.3.2: Strong Pearson's coefficient values for dimensional measurements. Correlations deemed strong between dimensional response variables and other response variables. Strong correlations existed between volume measurements and dimensional measurements. Other notable correlations were: Third metacarpal (MC3) width and proximal sesamoid bone (PSB) width; PSB length and PSB width; MC3 width and Trabecular Separation (Tb.Sp); MC3 width and Bone Volume Fraction (BV/TV); PSB width and Tb.Sp; and PSB length and Tb.Sp.

Parameter 1	Parameter 2	Correlation Coefficient
MC3 Width	TV	0.8794772
MC3 Width	BV	0.7717996
MC3 Width	Volume	0.8070864
MC3 Width	Tb.Sp	0.7916119
MC3 Width	BV/TV	-0.7360496
MC3 Width	PSB Width	0.8439014
PSB Width	TV	0.9124323
PSB Width	BV	0.8490894
PSB Width	Volume	0.8648942
PSB Width	PSB Length	0.7202423
PSB Width	Tb.Sp	0.8084853
PSB Length	TV	0.7994226
PSB Length	BV	0.8164543
PSB Length	Volume	0.8250549
PSB Length	Tb.Sp	0.7938988
PSB Length	PSB articular surface length (straight)	0.7043439
PSB depth @ articular bulge	TV	0.8593529
PSB depth @ articular bulge	BV	0.7911657

PSB depth @ articular bulge	Volume	0.7671142
PSB depth @ articular sulcus	TV	0.7973499
PSB depth @ articular sulcus	BV	0.7404271
PSB depth @ articular sulcus	Volume	0.7099088

2.3.2 Experiment 2: Clinical and Micro-Computed Tomography Structural Anatomy

Linear mixed model results are shown in Table 2.3.3 for μCT parameters and Table 2.3.4 for cCT parameters. Weight was a significant predictor for TV, BV, BV/TV, Conn.D, Tb.N, Tb.Th, DA, and Volume ($p < 0.05$), exhibiting a positive relationship with TV, BV, BV/TV, Tb.Th, DA, and Volume and a negative relationship with Conn.D and Tb.N. Sex was a significant predictor for TV only, with intact males having greater TV than female horses ($p < 0.05$). Age was a significant predictor for vBMD ($p < 0.05$), exhibiting a positive relationship. Leg was not a significant predictor for any structural parameters ($p > 0.05$). When comparing medial PSBs to lateral PSBs (Figure 2.3.3): Tb.Sp, DA, Volume, and vBMD were all parameters found to be greater in the medial PSB ($p < 0.05$).

Strong correlations between structural parameters were observed between size and volume parameters (Table 2.3.5). Notably, strong negative correlations were seen between BV/TV and Volume (Pearson's coefficient of -0.7005327), Conn.D (Pearson's coefficient of -0.7022588), and Tb.N (Pearson's coefficient of -0.9340619). Tb.Sp exhibited a strong positive correlation with Volume (Pearson's coefficient of 0.7961490). Conn.D was positively correlated with Tb.N (0.7729391). Tb.Th was strongly negatively correlated with Tb.N (Pearson's coefficient of -0.9381557) and strongly positively correlated to BV/TV (Pearson's coefficient of 0.9291446).

Table 2.3.3: Linear mixed model analysis of micro-computed tomography (μCT) response variables

A linear mixed model was used to compare predictor variables to μCT response variables. Weight was a positive predictor for Total Volume (TV), Bone Volume (BV), Bone Volume Fraction (BV/TV), Trabecular Thickness (Tb.Th), and Degree of Anisotropy (DA) and a negative predictor for Connectivity Density (Conn.D) and Trabecular Number (Tb.N) ($p < 0.05$). Gender was only a predictor for TV, with intact males exhibiting greater TV than females ($p < 0.05$). Medial proximal sesamoid bones (PSBs) exhibited greater Th.Sp and DA compared to lateral PSBs ($p < 0.05$). Age and forelimb was not a predictor for any μCT measurements ($p > 0.05$).

μCT Parameter	Comparison	P-value
TV	Age	0.1603106
	Weight–Positive relationship	0.0000000*
	Sex–Intact Male > Female	0.0236680*
	Bone	0.7999671
BV	Age	0.3525735
	Weight–Positive relationship	0.0000001*
	Sex	0.0946795
	Bone	0.7934295
BV/TV	Age	0.9391267
	Weight–Positive relationship	0.0126250*
	Sex	0.4653799
	Bone	0.4781696
Conn.D	Age	0.5886027
	Weight–Negative relationship	0.0011078*
	Sex	0.5955109
	Bone	0.2881613
Tb.N	Age	0.8865335
	Weight–Negative relationship	0.0004276*
	Sex	0.4767885
	Bone	0.8305564
Tb.Th	Age	0.6731488
	Weight–Positive relationship	0.0166007*
	Sex	0.4217579
	Bone	0.7934426
Tb.Sp	Age	0.1202146
	Weight	0.2221553
	Sex	0.2672231
	Bone–Medial PSB > Lateral PSB	0.0410771*
DA	Age	0.8809090
	Weight–Positive relationship	0.0484908*
	Sex	0.2767760
	Bone–Medial PSB > Lateral PSB	0.0377438*

Table 2.3.4: Linear mixed model analysis of clinical computed tomography (cCT) response variables

Linear mixed model comparison of predictor variables to cCT response variables. Age was a positive predictor for volumetric bone mineral density (vBMD, $p < 0.05$). Weight was a positive predictor for Volume ($p < 0.05$). Medial proximal sesamoid bones (PSBs) exhibited greater vBMD and Volume compared to lateral PSBs ($p < 0.05$).

cCT Parameter	Comparison	P-value
vBMD	Age Positive relationship	0.0268182*
	Weight	0.8513483
	Sex	0.3388371
	Leg	0.6494584
	Bone Medial PSB > Lateral PSB	0.0000277*
Volume	Age	0.1089917
	Weight Positive relationship	0.0006331*
	Sex	0.9092282
	Leg	0.9695103
	Bone Medial PSB > Lateral PSB	0.0106362*

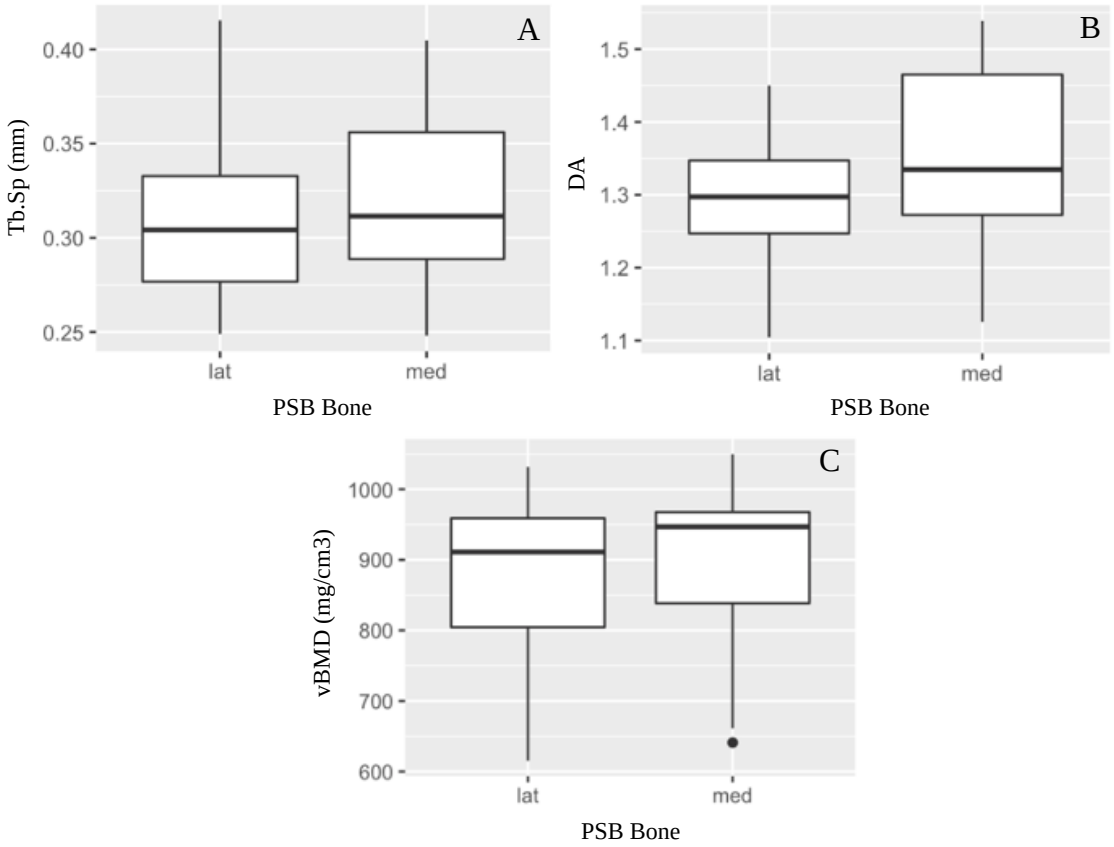

Figure 2.3.3: Box plots comparing significant medial-lateral structural differences
Medial proximal sesamoid bones (PSBs) were found to be significantly greater than PSBs for multiple structural parameters ($p < 0.05$). A. Trabecular separation was greater in medial PSBs than lateral PSBs ($p < 0.05$). B. Degree of Anisotropy was greater in medial PSBs than lateral PSBs ($p < 0.05$). C. Volumetric Bone Mineral Density was greater in medial PSBs than lateral PSBs ($p < 0.05$).

Table 2.3.5: Pearson's coefficient values for structural parameter measurements
Strong Pearson's correlations between parameters indicating size, including volume parameters, were observed. Notable correlations included: Bone Volume Fraction (BV/TV) and Volume; BV/TV and Connectivity Density (Conn.D); BV/TV and Trabecular Number (Tb.N); Trabecular Separation (Tb.Sp) and Volume; Conn.D and Tb.N; Trabecular Thickness (Tb.Th) and Tb.N; Tb.Th and BV/TV.

Parameter 1	Parameter 2	Correlation Coefficient
BV	Volume	0.9117589
BV/TV	Tb.Th	0.9291446
Conn.D	Tb.N	0.7729391
Conn.D	BV/TV	-0.7022588
Tb.N	BV/TV	-0.9340619
Tb.N	Tb.Th	-0.9381557
TV	BV	0.9667122
TV	Volume	0.9819325
Volume	Tb.Sp	0.7961490
Volume	BV/TV	-0.7005327

2.3.3 Experiment 3: Proximal Sesamoid Bone Maturation Timeline

When μCT parameters were graphed as a function of donor age, timelines of age-dependent changes in PSB structure become apparent. Nonlinear regression was used to fit an asymptotic exponential curve to determine an age-independent plateau point of stability if one was present. Table 2.3.6 lists the calculated age in days at which the different PSB structural parameters stabilized.

Conn.D and DA are both measures of trabecular arrangement. They both changed rapidly early in life and then quickly plateaud. Conn.D showed a rapid decrease and DA showed a rapid increase after birth. Conn.D and DA reached a plateau point within the first six months of life (Figure 2.3.4).

TV and BV, which calculate the total tissue and bone volume of the sample, respectively, and BV/TV, which indicates bone mineral density, all experienced a rapid

increase in early life that then leveled off. Tb.N, Tb.Th, and Tb.Sp all represent trabecular structure within the bone. Tb.N experienced a rapid decrease in early life before leveling off. Tb.Th and Tb.Sp increasd rapidly in early life. Tb.Th appeared to reach a plateau while Tb.Sp continued to increase. TV, BV, BV/TV, Tb.N, and Tb.Th reached a plateau point between six months and two years of life (Figure 2.3.5). Tb.Sp was the only parameter that did not plateau within the age range studied (Figure 2.3.6).

Though vBMD, a cCT measurement of bone mineral density, was not fit for an exponential function, it exhibited a similar pattern as other structural parameters, with a period of change before plateauing off (Figure 2.3.7).

Table 2.3.6: Calculated age at which proximal sesamoid bone (PSB) structural parameters stabilize.
Calculated ages at which steady state was reached within each micro-computed tomography (µCT) bone morphometry evaluation parameters measured for the proximal sesamoid bones, analyzed using an asymptotic exponential curve. All parameters with the exception of Trabecular Separation (Tb.Sp) appeares to reach an age-independent plateau prior to two years of age. Most notably, Connectivity Density (Conn.D) and Degree of Anisotropy (DA) plateaued within the first five months of life. Total Volume (TV), Bone Volume (BV), Bone Volume Fraction (BV/TV), Trabecular Number (Tb.N), and Trabecular Thickness (Tb.Th) reached a plateau between 6 and 24 months of age.

BME Parameter	Age at maturity	Age at maturity
BV	517 days	17 months
BV/TV	284 days	9.5 months
Conn.D	134 days	4.5 months
DA	52 days	1.5 months
Tb.N	366 days	12 months
Tb.Sp	3433 days	114.5 months
Tb.Th	691 days	23 months
TV	464 day	15.5 months

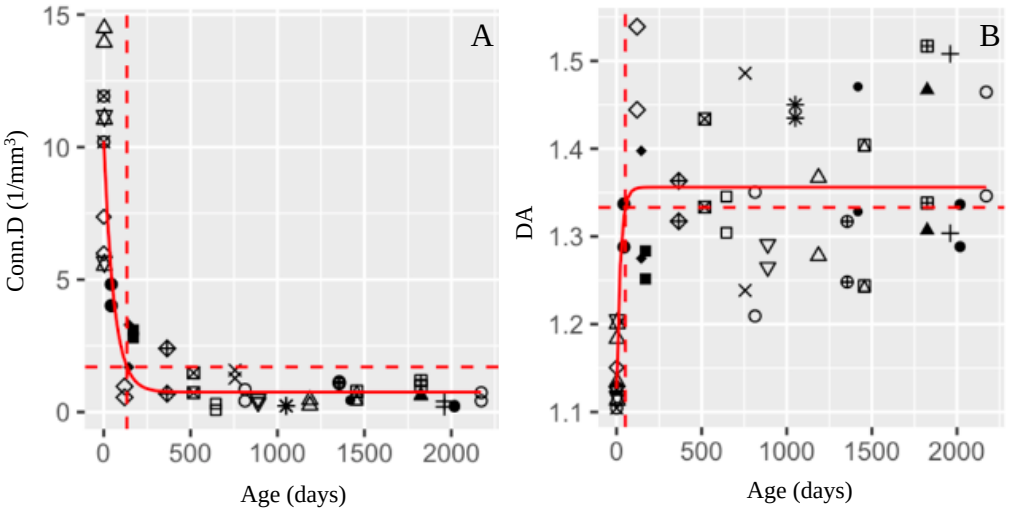

Figure 2.3.4: Micro-computed tomography (μCT) parameters Connectivity Density (Conn.D) and Degree of Anisotropy (DA) fit to an exponential curve

Micro-CT parameters Conn.D and DA were graphed against donor age with an asymptotic exponential function fit to determine the point of stabilization. The point of stabilization was determined as 90% of the difference of average initial value and average asymptotic (average maximum/minimum) value. A. Conn.D exhibited a clear and rapid decrease that then plateaued off at 4.5 months of age. B. DA exhibited a rapid increase early in life, with stability reached at 1.5 months. The age of stabilization was well within the first six months of life for both Conn.D and DA.

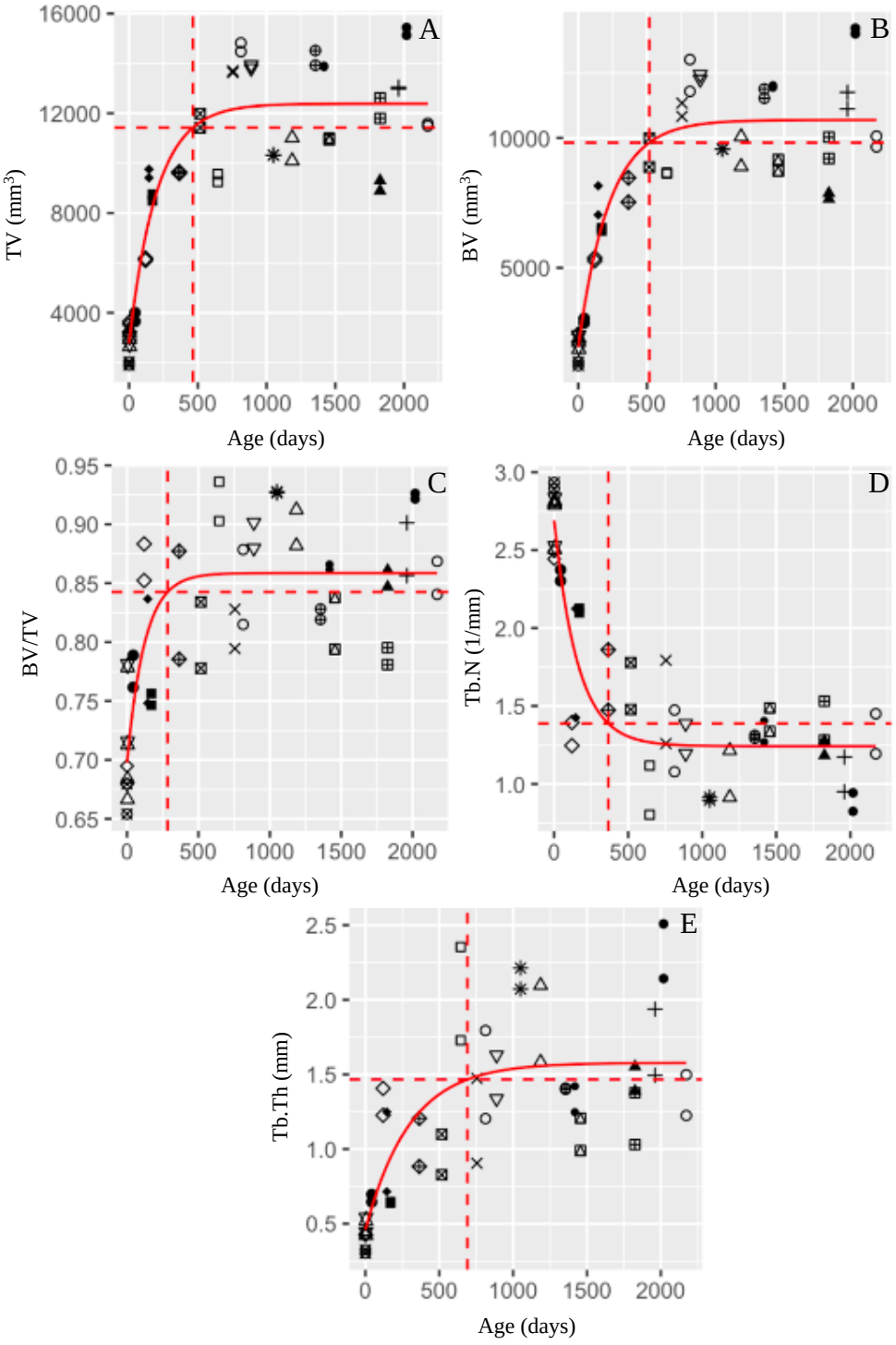

Figure 2.3.5: Micro-computed tomography (µCT) parameters Total Volume (TV), Bone Volume (BV), Bone Volume Fraction (BV/TV), Trabecular Number (Tb.N), Trabecular Thickness (Tb.Th) fit to an exponential curve

Micro-CT parameters TV, BV, BV/TV, Tb.N, and Tb.Th were graphed against donor age with an asymptotic exponential function fit to determine the point of stabilization. The point of stabilization was determined as 90% of the difference of average initial value and average asymptotic (average maximum/minimum) value. A. TV exhibited a clear and rapid increase with a plateau observed at 15.5 months. B. BV also underwent a clear and rapid increase. The PSBs plateaued at 17 months of age. C. BV/TV reached stability in the PSBs by 9.5 months, exhibiting a similar increase as BV and TV. D. Trabecular Number (Tb.N) showed a rapid decrease and then plateaued at one year of age. E. Trabecular Thickness (Tb.Th) showed an increase until stability at 23 months of age. These calculated ages at stabilization all occurred within the first 24 months of life.

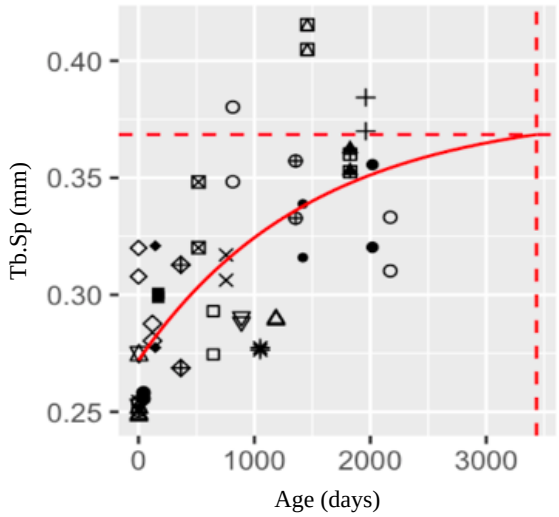

Figure 2.3.6: Micro-computed tomography (μCT) parameter Trabecular Separation (Tb.Sp) fit to an exponential curve

Micro-CT parameter Tb.Sp was graphed against donor age with an asymptotic exponential function fit to determine the point of stabilization. The point of stabilization was determined as 90% of the difference of average initial value and average asymptotic (average maximum/minimum) value. Tb.Sp did not exhibit a plateau within the age range studied, though an increase is observed. The age at stability was estimated to be roughly 9.5 years of age.

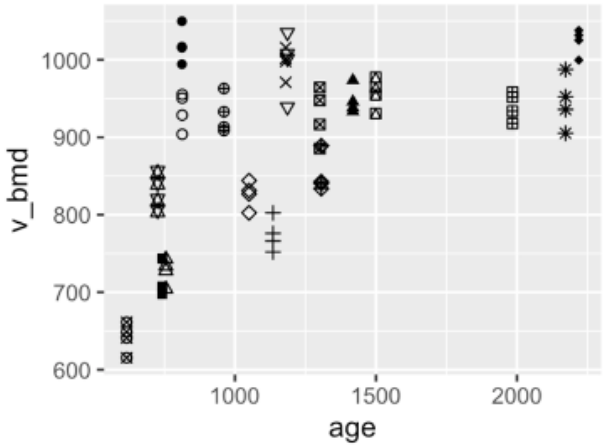

Figure 2.3.7: Clinical computed tomography (cCT) parameter Volumetric bone mineral density (vBMD) graphed against donor age
Volumetric BMD, a cCT parameter, exhibited an increase over the age range studied. A similar pattern was observed to many micro-computed tomography parameters, where an initial increase was followed by a plateau.

2.4 Discussion

The data demonstrate a clear positive relationship between donor weight and most dimensional and structural parameters, supporting the understanding that bones typically increase in size with body weight during the period of growth and maturation of an animal. Differences were also observed for dimensional and structural parameters between medial and lateral PSBs within the forelimb of our sample population.

2.4.1 Experiment 1: Proximal Sesamoid Bone Dimensional Measurements

Data on the changes of anatomical and structural parameters in forelimb PSBs and their relation to dimensional measurements of the distal MC3 within ‘population normal’ Thoroughbreds were investigated in the postnatal period between birth and six years of age. No PSB dimensional measurements were significantly different between the LF and RF limbs. In contrast, differences between the medial and lateral PSBs were observed. The

lateral PSB length was greater than medial PSB length. PSB depth was observed to be greater in medial PSB than lateral PSB. Medial PSB width was not significantly greater than lateral PSBs; however, it is approaching significance raising the possibility that the study may have been underpowered to assess the width parameter. The current findings are consistent with previously reported information that lateral PSBs are longer than medial PSBs.[4,45,46] The significant comparison of medial and lateral PSBs depth at the articular bulge of MC3, with the medial PSB being great than the lateral PSBs, was in contrast with Alrtib et al. (2013).[45] PSB width being not significantly different between LF and RF limb, nor between medial PSB vs lateral PSBs, contradicts previous findings by Anthenill et al. (2006); however, these findings on medial vs lateral PSB width are consistent with what was observed by Alritb et al. (2013).[4,45]

Strong correlations observed between distal MC3 width and PSB width and between PSB width and PSB length are consistent with the close anatomical relationship between these two bones. This relationship is likely also important for the normal biomechanical function of the equine MCP joint. Strong correlations were also observed between dimensional measurements and structural parameters. There exists a positive correlation between Tb.Sp of the PSBs and MC3 width, PSB width, and PSB length, indicating that as PSB size increases, spacing between trabeculae increases. This finding is reflected in the negative correlation observed between distal MC3 dimensions and the BV/TV of PSBs. So, on average, horses with larger cannon bones will have larger PSBs, but those PSBs will have a lower BV/TV (i.e. lower density). The strong correlations observed between dimensional measurements and structural parameters of PSB volume are expected, as they are all measurements of bone size. On a functional level, having

anatomically appropriate size relationships would be necessary for the even distribution of forces between MC3 condyles and PSBs, achieving optimal biomechanical relationships within the MCP joint. [50,51,70]

2.4.2 Experiment 2: Clinical and Micro-Computed Tomography Structural Anatomy

The observed relationships between weight and multiple PSB structural parameters as measured by both μCT and cCT are fully consistent with skeletal growth and bone modeling during maturation–as horses increase in body size, the bones grow and mature as well. The positive relationship between age and vBMD also can be explained by normal growth and modeling, with BMD increasing as bone maturation progresses and the mineral content of the bone increases. Notably, no effect was seen on vBMD based on right or left limb. This suggests that even though North American Thoroughbred racehorses usually travel counterclockwise on racetracks for high speed exercise and competition, the LF and RF fetlock joints do not experience different biomechanical forces. Changing leads at the asymmetrical gallop during high speed exercise is almost certainly an important part of achieving this balance. More investigation is needed to determine if forelimb structural differences exist for μCT BME parameters.

On the other hand, structural differences between the medial and lateral PSBs were consistently observed for Tb.Sp, DA, and vBMD, with medial PSBs having greater values than lateral PSBs ($p < 0.05$). These differences can be attributed to the normal anatomy of the MCP joint. The medial condyle of the MC3 has been reported to be larger than the lateral condyle.[45] Liley et al. (2018) reported that an increased area of the lateral condyle (decreasing variation between the medial and lateral condyles) of the distal MC3 was coupled with decreased BMD values across the entire distal MC3.[70] Liley et al. (2018) did

not investigate the PSBs.[70] Decreased variation between the medial and lateral condyles of the distal MC3 would lead to a change in biomechanical forces traveling through the PSB, with a more even distribution of forces between the condyles and PSBs of the MCP joint.[50,51,70] Since MC3 medial condyles within these "population normal" horses are presumed to be greater than the lateral condyles, this would indicate the medial PSB experiencing more force, causing the BMD to be greater in the medial PSB compared to the lateral PSB. [50,51,70] This study also found the medial PSB to be significantly deeper at the articular bulge of MC3 than the lateral PSB, which would cause similar biomechanical changes and increase force distribution.

The observation that medial PSBs DA is greater than lateral PSBs is not consistent with the report by Cresswell et al (2019), where no differences were observed.[8] This may reflect differences between the two sample sets, but will be an important issue to clarify to facilitate interpretation of PSB structural data from racehorses suffering serious injuries of the suspensory apparatus.

2.4.3 Experiment 3: Proximal Sesamoid Bone Maturation Timeline

Determining the relationship between PSB structural parameters and Thoroughbred age has important relevance to the debate on what age is appropriate for Thoroughbred horses to enter high speed training and competition. The current data documented substantial and often rapid changes in the postnatal period through approximately 23 months of age, but then a plateau and stabilization of parameters was observed out to six years. DA and Conn.D exhibited rapid change within the first six months of life, with plateau points of 52 days and 134 days, respectively. This short timescale suggests that changes in these parameters reflect the major transitions a foal experiences transitioning

from a non-weight-bearing aqueous environment *in utero* to postnatal weight-bearing and ambulation. In contrast, the parameters TV, BV, BV/TV, Tb.N, and Tb.Th all increase over a more extended time frame, with the horizontal age-independent asymptote (placed at 90% the average maximum or minimum values) reached between six months of age and two years of age. Thus, changes in these parameters likely reflect skeletal growth and maturation variables of the equine lower limb. Importantly, the data are consistent with two-year-old Thoroughbreds having mature appendicular skeletal structure upon entering high speed training in preparation for racing competition, at least in the context of PSB biology.

Tb.Sp was the only PSB structural parameter that did not exhibit a well-defined plateau point within the age range studied. The data indicate that trabecular spacing continues to increase past six years of age. Interestingly, and fully consistent, Babiarz (2021, in preparation) observed that age was a significant predictor variable only for Tb.Sp in Thoroughbreds aged 21 months to 71 months.[71] This raises the possibility that trabecular spacing is an important variable not only for growth and maturation, but also for PSB modeling later in life due to changes in biomechanical forces associated with high-speed training and horseracing competition. Volumetric BMD was not fitted for an asymptotic exponential curve, so a point of stabilization could not be determined. However, the graph appears to display a similar pattern of rapid increase followed by a slower rise to the upper limit of subject ages, consistent with BMD also being an important parameter in racehorse PSB modeling.

A greater understanding of the PSB maturation timeline in Thoroughbreds has been achieved, with most structural parameters from the μCT and cCT data showing

stabilization by 24 months of age. Preliminary data on normal levels of variation between individual horses for PSB anatomical and structural parameters has been established for Thoroughbreds between birth and six years of age. Differences between medial and lateral PSB anatomical and structural parameters have also been demonstrated that appear consistent with distal MC3 dimensions and relationships with the MCP joint.

2.4.4 Limitations of this study

The sample population was limited to Kentucky Thoroughbred foals and racehorses that were collected between 2015 and 2021. Due to the objectives of Thoroughbred breeders and owners, it was not logistically feasible to collect a PSB sample set composed only of horses who had no training, either for racing or other athletic pursuits. Due to a limited population sample size, there was limited ability to age and gender match the sample set used for this study. Not all samples within the sample set were able to be scanned by both μCT and cCT, as the collaboration that enabled cCT data collection did not start until 2019 when the cCT instrument first became available. With regard to μCT data, only LF PSB images were analyzed, preventing comparisons between the two forelimbs.

CHAPTER 3. CONCLUSIONS

3.1 Reflection

Because of its prevalence in racing populations, a great deal of research is being done to understand the etiology and pathogenesis of PSB fracture and suspensory apparatus failure in racehorses.[8,9,10,11] Most of the present research investigating PSBs is being completed on racing Thoroughbreds with the goal of understanding PSB breakdown mechanics.[8,9,10,11] There is little known about their normal maturation, structural anatomy, and population variation. The limited information that has been reported is that PSB ossification begins between 290 and 330 days gestation, with complete ossification occurring around three to four months post parturition.[68,69] While a more in-depth investigation into the developmental process is important, this study focused on filling the knowledge gap in the PSB maturation timeline starting at birth through six years of age. Data representing race aged horses that can be considered normal population, i.e. without musculoskeletal pathology, is limited.[8,9,10,11] This prevents proper interpretation of results and analysis of pathology when investigating PSB breakdowns, since differences that may simply reflect age, gender, size, or inter-animal variation cannot currently be taken into consideration.

3.1.1 Purpose

The goal of this study was to fill the knowledge gap surrounding PSB maturation and normal population variation by providing normalized baseline anatomical and structural data for PSBs in healthy Thoroughbred horses. This includes investigation into the maturation timeline from birth through six years of age and normal levels of variation

between race aged individuals. The research question addressed was whether anatomical and structural parameters of PSB maturation have gender-dependent differences and correlate with third metacarpal (MC3) medial-lateral width at the metacarpophalangeal (MCP, fetlock) joint.

3.1.2 Methods

Anatomical and structural parameters of PSB maturation were investigated using clinical computed tomography (cCT) and micro-computed tomography (μCT) in Thoroughbred horses aged zero days to six years of life. Thirty-six Thoroughbred horses within the age range were collected postmortem form University of Kentucky Veterinary Diagnostic laboratory. Fourth-eight PSBs form 24 horses aged zero to six years of age were analyzed via μCT Bone Morphometry Evaluation (BME) for structural parameters of bone. Seventy-two PSBs from 18 horses were evaluated using cCT through dimensional measurements and Bone Mineral Density (BMD) testing. A linear mixed model was used to evaluate both μCT and cCT results. Nonlinear regression was used to fit an asymptotic exponential function to the μCT BME output data to determine if a point (i.e. age) existed within the timeline of ages investigated where the parameter stabilized (plateaued).

3.1.3 Results and implications

Medial versus lateral PSB differences were clearly seen for multiple parameters, both for dimensional measurements and structural parameters. Medial PSBs were observed to be shorter than lateral PSBs, which confirmed previous findings.[4,45] Medial PSBs were observed to be deeper than lateral PSBs, a finding in contrast to an earlier study that reported lateral PSBs being deeper than medial PSBs.[45] Medial PSBs were greater in

Tb.Sp, DA, Volume, and vBMD than lateral PSBs. It has previously been reported in the MC3 condyles that BMD is higher in larger bones.[70] The greater volume within the medial PSB explains the increased BMD compared to the lateral PSB. This size difference may also explain the structural differences seen, as greater force traveling through the larger medial MC3 condyle and PSB might result in increased DA and Tb.Sp due to the increased load experienced compared to the lateral PSB.[43] Currently, no differences were seen in dimensional measurements or cCT parameters between left forelimb and right forelimb, indicating that the forelimbs mature similarly and experience similar biomechanical forces in a normal population. More investigation is needed to determine if limb differences exist for μCT parameters.

Age-dependent plateau points were clearly seen in multiple μCT BME parameters, including TV, BV, BV/TV, Conn.D, Tb.N, Tb.Th, and DA. Conn. D and DA experiences highly rapid change within few months of life, with the point of stabilization occurring well within six months of age. This finding was interpreted as likely reflecting the change from non-weight-bearing *in utero* existence to postnatal weight-bearing within hours of birth. TV, BV, BV/TV, Tb.N, and Tb.Th also exhibited substantial age-dependent changes, but with an extended timeline. For each of these parameters, the point of stabilization occurred between nine and 23 months. These changes seem more consistent with skeletal growth and maturation, together with biomechanical loading forces associated with non-equestrian activity. The observation seems relevant to debates between members of the racing industry and the public centered on whether two-year-old Thoroughbreds are anatomically and physiologically mature enough for high speed race training and competition. These PSB data indicate that “yes,” they are ready.

3.2 Additional Questions for the Data Set

Histologic analyses may provide additional relevant data regarding the timeline of PSB maturation. This includes differences in cell composition between certain timepoints, such as at birth compared to when Thoroughbreds start training, and precise timepoints for major events in maturation, such as when ossification is initiated and completed and when hypertrophy of cells is complete

Investigation into the regional differences will reveal the location of the PSB ossification center and aid in understanding fracture mechanics. PSB fractures occur more often in the apical region of the bone compared to the midbody and basilar regions of the bone.[6] Understanding if regional differences exist within the PSBs, and perhaps between individuals within the normal population would be interesting. Such associations have the potential to help elucidate fracture mechanics and identify risk susceptibilities for PSB fracture.

3.3 New and High Priority Questions

One question which remains, which would provide insight not only into PSB fracture mechanics, but also provide insight into other CMI injuries of the MCP joint, is the interconnected nature of anatomy and physiology within the MCP joint. The MCP joint experiences the most force during the stance phase of locomotion, while the suspensory apparatus stores and releases energy during the cycle of locomotion to decrease the energy expenditure of the horse.[47,48,49] When in the stance phase, the suspensory apparatus causes displacement of the PSBs and articulation between the condyles of MC3 and the PSB articular surface[47]. The resulting stress occurs from the antiparallel force created by the

attached ligaments, as well as the contact force created between the articular surfaces of the PSBs and the MC3.[50] The traditional ideology surrounding PSB fracture is that a "bad step" during racing or training generated a sudden extreme biomechnical overload resulting in structural failure. However, the current PSB fracture model reflects a final macro structural failure after the accumulation of micro damage created by loading forces that are experienced by the suspensory apparatus, and the embedded PSBs, during locomotion.[48,50,51,72] Assuming this model is correct, PSB fracture is an instance when form (i.e. internal structural anatomy) is unable to adapt (i.e. modeling) to the function of the bone (i.e. increase strain during high speed exercise), resulting in failure. While this study has provided preliminary data for the PSBs, and BMD has been investigated in the MC3, further study into structural anatomy for all components of the MCP joint is needed to more fully understand the changes resulting from high speed exercise that can lead to CMI. Utilizing dimensional measurements and cCT and μCT structural parameters to investigate the entirety of the MCP joint, including MC3, P1, and PSBs, would elucidate any effects existing between the four main bony elements of the joint, including effects seen on gross anatomy, internal structural anatomy, and biomechanics. In other words, anatomical components of the MCP joint need to be considered together.

Skeletal development is a fundamental process that has been established in long bones, but which remains opaque for sesamoid bones for all species. Understanding the development of the PSBs can lead to better understanding of the PSBs a whole, including maturation, response to exercise and loading, and fracture mechanisms. Despite PSB injuries having major epidemiological significance in CMI of racehorses, knowledge on the embryonic and fetal development of these bones is limited, with only two published

sources located.[68,69] The information reported is that equine PSBs begin ossification *in utero* at 290-330 days, with initial mineral deposition being observed from a single ossification center.[68,69] One source goes on to state that ossification is completed after parturition, by three to four months of age, though the size of the PSBs may increase until 18 months of age.[69] This ossification timeline differs slightly from what is observed in humans, where cartilaginous sesamoids do not commence ossification until early childhood and is final in late adolescence or early adulthood.[65,58,55,66,67] However, perhaps perinatal ossification should not be unexpected in ungulates, which must stand up and achieve the ability to ambulate at relatively high speeds within hours of birth.

Details of early fetal development of sesamoid bones are also important question. A long standing and widely accepted model of development is that sesamoid bones develop within a tendon separate from the long bones of a joint in response to fetal movement.[53,54,55] However, new models for development are emerging as cell signaling pathways are elucidated, suggesting sesamoid bones may originate from the long bones of a joint.[61,62] While the exact machination of sesamoid bone development may be disputed, there is clear evidence suggesting endochondral bone formation with both mechanical and genetic contributions.[60,63,64] While little is known about the development of the cartilaginous sesamoid bones in horses prior to the start of ossification, there has been evidence of cell aggregation forming at the sight of PSB development as early as day 46 in gestation (Adam, Lowney & MacLeod – unpublished). There still exists a tremendous amount of knowledge about sesamoid bones across all species which remains unknown at this time. The study of both fetal and postnatal PSB development within the horse could help elucidate developmental pathways across various species.

The generation of population databases following horses from inception of training through their racing career, including the individual horse's history on racing, injury, and radiographs taken such as x-ray, CT, and PET scans, would allow investigators to note any changes or abnormalities which existed prior to CMI. These abnormalities can then be flagged when appearing on racing horses' radiograph images and mark a horse for having an increased risk of injury. This would also provide a large backlog of data for horses considered population normal, providing in depth population variation data. These data would greatly enhance the investigation of PSB breakdown injuries, as it currently cannot be explicitly determined if changes are due to pathology or if these are normal changes seen across the entire racing population. A large database of both normal and abnormal images would also provide the potential for possible machine learning, allowing the computer to analyze and determine risk at greater accuracy than the trained human eye. Machine learning is becoming more prevalent in the medical field due to artificial intelligence advancement. With these advancements, computers are able to recognize abnormalities which they are "taught" through annotation of files. However, machine learning advancements can only be utilized with the generation of these population databases where large collection of files can be annotated for pathology.

APPENDICES

APPENDIX 1: ABBREVIATIONS

App Table 1 below contains all abbreviations used in this work.

App Table 1: Table displaying all abbreviations used within this work alphabetically.

Abbreviation	Meaning
aBMD	areal bone mineral density
BMD	bone mineral density
BME	bone morphometry evaluation
BMP	bone morphogenic factor
BV	bone volume
BV/TV	bone volume fraction
cCT	clinical computed tomography
CMI	catastrophic musculoskeletal injury
Conn.D	connectivity density
CT	computed tomography
DA	degree of anisotropy
DDFT	deep digital flexor tendon
FGF	fibroblast growth factor
IM	interosseous muscle
LF	left front limb
LH	left hind limb
LRS	lactated ringers solution
MC3	third metacarpal bone
MCP	metacarpophalangeal joint
MRI	magnetic resonance imaging
MTP	metatarsophalangeal joint
NMR	nuclear magnetic resonance, another term for MRI
P1	first phalanx
PET	positron emission tomography
PSB	proximal sesamoid bone
RF	right front limb
RH	right hind limb
ROI	region of interest
SDFT	superficial digital flexor tendon
Tb.N	trabecular number
Tb.Sp	trabecular separation

Tb.Th	trabecular thickness
TV	total volume
vBMD	volumetric bone mineral density
VDL	veterinary diagnostic laboratory
X-ray	x-radiation imaging
µCT	micro-computed tomography

APPENDIX 2: POPULATION SPECIFICS

Seventy-two horses ages 0 to 536 days old were collected for this study from the University of Kentucky Veterinary Diagnostic Laboratory (VDL). Pathologies were determined for all available specimens and then classified by diagnosis and organ system, with their effect on fetal growth rate and bone maturation determined. Horses diagnosed with pathology with known effects on bone development and maturation were excluded. Out of the remaining specimens with no effect on development or maturation, 10 were selected which had no pathology of the fetlock joint and aged 0 days to 516 days old. All 10 horses were used for μCT investigation only.

Five horses aged two years to five years old were donated by owner elected euthanasia to the University of Kentucky Gluck Equine Research Center for research purposes. One horse was excluded due to osteopenia in the entirety right front limb caused by previous injury resulting in non-weight-bearing for a prolonged period of time. Four horses aged two years to five years of age were considered normal population and used within the sample population. One horse was used in both μCT and cCT investigation and three horses were used only in μCT investigation.

Eighty-seven race age horses (two years to seven years old) that died at Kentucky race tracks were released to the University of Kentucky VDL per a Kentucky Racing Commission mandate. Upon necropsy, 22 horses aged two to six years were found to have died from injuries not relating to musculoskeletal injury and were deemed normal population. Five of these horses were used for both μCT and cCT investigation, five were

used only for μCT investigation, and 12 samples were used only for cCT investigation only.

Pathology for all selected samples are listed in App Table 2.

App Table 2: Present pathologies in all samples within the studied sample set.

Sample	Pathology
1	Perinatal death; Dysotica
2	Stillbirth; Dystocia
3	Dystocia; Fractured ribs; Hemothorax; Pulmonary lacerations
4	Small intestinal volvulus
5	Severe, multifocal perforating and non-perforating gastric ulcers; Severe, diffuse, necrotizing duodenitis; Focally extensive diaphragmatic hernia; Mild, multifocal, pulmonary granulomas
6	Suspect lightning strike
7	Coronary artery anomaly; mitral valvular endocarditis
8	Rhodococcus equi pelvic osteomyelitis and myositis
9	Acute necrotizing pneumonia and lymphadenitis (intermandibular, pharyngeal), *Streptococcus zooepidemicus, Staph aureus;* Intravascular thrombosis (kidney, liver, colon); Potomac Horse Fever – PCR positive
10	Cervical spina degenerative joint disease, C5-6; Severe cervical spinal axonal degeneration
11	Pulmonary artery rupture; Hemopericardium; Pulmonary artery degeneration and mineralization
12	Typhlocolitis
13	Brain and cervical spinal cord meningeal hemorrhage – presumed trauma
14	Mixed bacterial pleuritis
15	Control
16	Barn area trauma – basophenoid fx
17	Barn area trauma – undetermined – suspect acute, severe concussive event. No fractures were observed
18	EPM; Necrohemorrhage right dorsal colitis
19	Undetermined – acute collapse
20	Sudden death – undetermined cause of death
21	Multifocal myocardial fibrosis
22	Suppurative tubulointerstitial nephritis and pulmonary hemorrhage; RF lateral PSB apical fracture
23	Tension pneumothorax; Chronic myofasciitis (accident on racetrack)
24	Laminitis; Scrotal cellulitis
25	Stall accident – traumatic tongue laceration
26	Basisphenoid fracture with intracranial hemorrhage
27	Hemoperitoneum
28	Control
29	Hemoperitoneum

30	Control
31	Control
32	Subcutaneous hemorrhage and edema
33	Large colon volvulus
34	Colic – large colon displacement
35	Saddling Paddock Injury – skull fracture
36	Massive pulmonary hemorrhage

APPENDIX 3: ADDITIONAL DATA

A strong correlation was seen between the straight articular surface length and the curved articular surface length (Pearson's coefficient of 0.9964972), which was expected. While age is not a specific predictor, curved PSB articular surface length increases across the age range of 21 months to six years (App Figure 1). Weight is a positive predictor ($p < 0.05$, App Table 3). No other predictive variables, sex, forelimb, or bone, showed a relationship to articular surface length, indicating that body size is an important driver in PSB length.

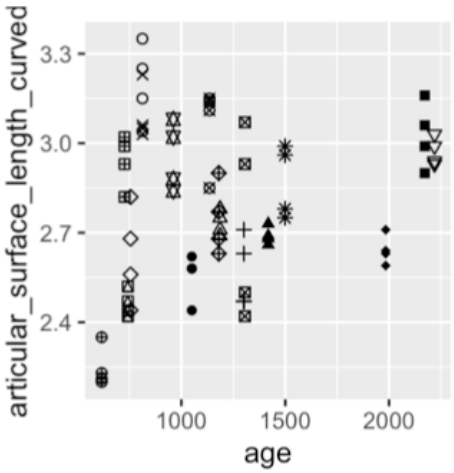

App Figure 1: Curved articular surface length appears to show an increase over the studied age range, though age at this time was not a significant predictor. Curved articular surface length of the PSB was shown to have a positive relationship with weight.

App Table 3: All comparisons between predictor variables and PSB curved articular surface length. At this time, weight is the only significant predictor ($p < 0.05$).

Dimensional Parameter	Comparison	P-value
PSB curved articular surface length	Age	0.0527704
	Weight–Positive relationship	0.0372821*
	Sex	0.3896448
	Leg	0.9327105
	Bone	0.9327105

A strong correlation (Pearson's coefficient of 0.8686516) exists between vBMD and BMD. aBMD shows a similar increase with age as vBMD (App Figure 2). However, aBMD was still observed to have both age and bone differences, with age showing a positive relationship to aBMD and the medial PSB having greater aBMD than the lateral PSB ($p < 0.05$, App Table 4). This same pattern is observed with vBMD. Mass showed the same relationships with age and bone, but also displayed a positive relationship with weight ($p < 0.05$). Looking at area, lateral PSBs had greater area compared to medial ($p < 0.05$); however, they displayed the same positive relationship with weight as Mass ($p < 0.05$). Upon consultation with Mindways Software support, vBMD was determined to be superior to aBMD for whole bone analysis due to less variation in volume measurements when placing the ROI around the bone (J. Brown).

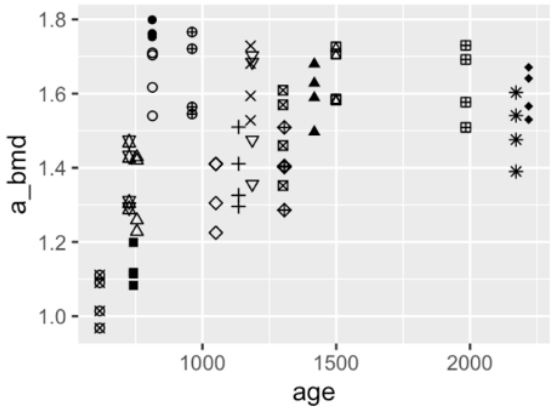

App Figure 2: aBMD shows an age related increase within the age range study consistent with what is seen with vBMD.

App Table 4: Age is a positive predictor variable for aBMD and Mass of the PSBs ($p < 0.05$). Weight is a positive predictor for Area and Mass of the PSBs ($p < 0.05$). Medial PSB were seen to have greater aBMD and Mass, while lateral PSBs were shown to have greater Area.

cCT Parameter	Comparison	P-value
aBMD	Age–Positive relationship	0.0216296*
	Weight	0.2035683
	Sex	0.2733501
	Leg	0.3667377
	Bone–Medial PSB>Lateral PSB	0.0106362*
Area	Age	0.0666626
	Weight–Positive relationship	0.0023378*
	Sex	0.8860554
	Leg	0.2279582
	Bone–Lateral PSB>Medial PSB	0.0000000*
Mass	Age–Positive relationship	0.0240516*
	Weight–Positive relationship	0.0236557*
	Sex	0.5783101
	Leg	0.9953832
	Bone–Medial PSB>Lateral PSB	0.0000126*

App Figure 3: Medial PSBs have greater aBMD and Mass values than lateral PSBs, while lateral PSBs have greater Area values than lateral PSBs.

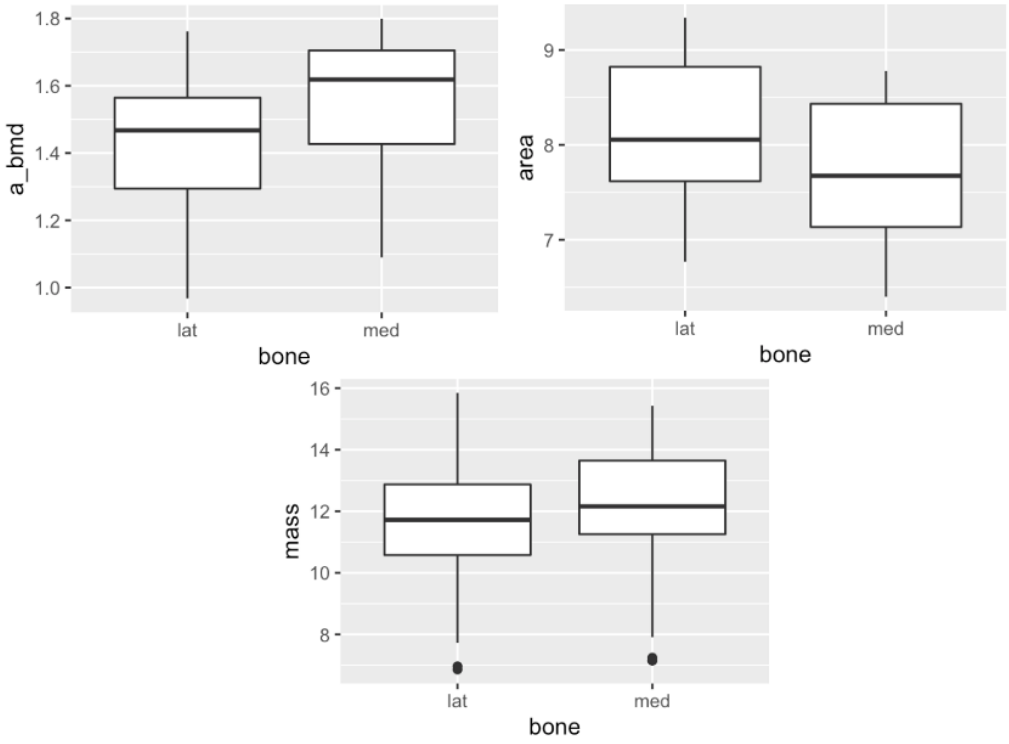

REFERENCES

1. Jeffcott, L. B., Rossdale, P. D., Freestone, J., Frank, C. J. & Towers-Clark, P. F. An assessment of wastage in Thoroughbred racing from conception to 4 years of age. *Equine Veterinary Journal* **14**, 185–198 (1982).
2. Hernandez, J., Hawkins, D. L. & Scollay, M. C. Race-start characteristics and risk of catastrophic musculoskeletal injury in Thoroughbred racehorses. *Journal of the American Veterinary Medical Association* **218**, 83–86 (2001).
3. The Jockey Club Releases Data from the Equine Injury Database for 2020. *The Jockey Club* http://jockeyclub.com/default.asp?section=Resources&area=10&story=1258 (2021).
4. Anthenill, L. A. *et al.* Association between findings on palmarodorsal radiographic images and detection of a fracture in the proximal sesamoid bones of forelimbs obtained from cadavers of racing Thoroughbreds. *Am J Vet Res* **67**, 858–868 (2006).
5. Johnson, B. J. *et al.* Causes of death in racehorses over a 2 year period. *Equine Veterinary Journal* **26**, 327–330 (1994).
6. Schnabel, L. V. & Redding, W. R. Diagnosis and management of proximal sesamoid bone fractures in the horse. *Equine Vet Educ* **30**, 450–455 (2018).
7. Reesink, H. L. Foal Fractures: Osteochondral Fragmentation, Proximal Sesamoid Bone Fractures/Sesamoiditis, and Distal Phalanx Fractures. *Veterinary Clinics of North America: Equine Practice* **33**, 397–416 (2017).
8. Cresswell, E. N., McDonough, S. P., Palmer, S. E., Hernandez, C. J. & Reesink, H. L. Can quantitative computed tomography detect bone morphological changes associated with catastrophic proximal sesamoid bone fracture in Thoroughbred racehorses? *Equine Veterinary Journal* **51**, 123–130 (2019).
9. Hill, A. E., Gardner, I. A., Carpenter, T. E. & Stover, S. M. Effects of injury to the suspensory apparatus, exercise, and horseshoe characteristics on the risk of lateral condylar fracture and suspensory apparatus failure in forelimbs of Thoroughbred racehorses. *American Journal of Veterinary Research* **65**, 1508–1517 (2004).
10. Anthenill, L. A., Stover, S. M., Gardner, I. A. & Hill, A. E. Risk factors for proximal sesamoid bone fractures associated with exercise history and horseshoe characteristics in Thoroughbred racehorses. **68**, 12 (2007).
11. Shaffer, S. K. *et al.* Subchondral focal osteopenia associated with proximal sesamoid bone fracture in Thoroughbred racehorses. *Equine veterinary journal* **53**, 294–305 (2021).
12. Young, A. Imaging. *UC Davis School of Veterinary Medicine* https://ceh.vetmed.ucdavis.edu/imaging (2019).
13. Cierniak, R. Some Words About the History of Computed Tomography. in *X-Ray Computed Tomography in Biomedical Engineering* 7–19 (Springer London, 2011). doi:10.1007/978-0-85729-027-4_2.
14. X-rays. https://www.nibib.nih.gov/science-education/science-topics/x-rays.
15. Magnetic Resonance Imagining (MRI). *NC State University College of Veteirnary Medicine: Equine Orhtopedic Research Laboratory* https://projects.ncsu.edu/project/cvm-eqorth/MRI.html.
16. Geva, T. Magnetic Resonance Imaging: Historical Perspective. *Journal of Cardiovascular Magnetic Resonance* **8**, 573–580 (2006).

17. Gonzalez, L. M., Schramme, M. C., Robertson, I. D., Thrall, D. E. & Redding, R. W. MRI Features of Metacarpo(tarso)phalangeal Region Lameness in 40 Horses: MRI features of MP region lameness in 40 horses. *Veterinary Radiology & Ultrasound* **51**, 404–414 (2010).
18. Murray, R. C., Branch, M. V., Tranquille, C. & Woods, S. Validation of magnetic resonance imaging for measurement of equine articular cartilage and subchondral bone thickness. *American Journal of Veterinary Research* **66**, 1999–2005 (2005).
19. Dyson, S. & Murray, R. Use of concurrent scintigraphic and magnetic resonance imaging evaluation to improve understanding of the pathogenesis of injury of the podotrochlear apparatus. *Equine Veterinary Journal* **39**, 365–369 (2007).
20. Position Emission Tomography (PET). *NIH Clinical Center* https://clinicalcenter.nih.gov/pet.
21. Rich, D. A. A Breif History of Positron Emission Tomography. *Jounral of Nuclear Medicine Technology* **25**, 4–11 (1997).
22. Spriet, M. *et al.* ^{18} F-sodium fluoride positron emission tomography of the equine distal limb: Exploratory study in three horses. *Equine Vet J* **50**, 125–132 (2018).
23. Tietje, S., Becker, M. & Böckenhoff, G. Computed tomographic evaluation of head diseases in the horse: 15 cases. *Equine Veterinary Journal* **28**, 98–105 (1996).
24. Vanschandevijl, K. *et al.* Computed tomography–guided brain biopsy for in vivo diagnosis of a cholesterinic granuloma in a horse. *Journal of the American Veterinary Medical Association* **233**, 950–954 (2008).
25. Lacombe, V. A., Sogaro-Robinson, C. & Reed, S. M. Diagnostic utility of computed tomography imaging in equine intracranial conditions: CT imaging and intracranial conditions. *Equine Veterinary Journal* **42**, 393–399 (2010).
26. Tucker, R. L. & Sande, R. D. Computed Tomography and Magnetic Resonance Imaging in Equine Musculoskeletal Conditions. *Veterinary Clinics of North America: Equine Practice* **17**, 145–157 (2001).
27. Vekens, E. V. der *et al.* Computed tomographic anatomy of the equine stifle joint. *American Journal of Veterinary Research* **72**, 512–521 (2011).
28. Huang, K. *et al.* Impact of slice thickness, pixel size, and CT dose on the performance of automatic contouring algorithms. *Journal of Applied Clinical Medical Physics* **22**, 168–174 (2021).
29. OsiriX DICOM Viewer | Company. https://www.osirix-viewer.com/about/company/.
30. Bone Investigational Toolkit, QCT Pro Plus, Mindways Software INC. https://www.qct.com/QCTProPlus.html.
31. QCT Pro Bone Investigaion Toolkit User's Guide. (2006).
32. QCT Pro Bone Mineral Density Software Report Content and Interpreation Module. (2011).
33. Bone Density. *NIH U.S. National Librayr of Medicine: MeSH* https://meshb.nlm.nih.gov/record/ui?name=Bone%20Density.
34. Cornelissen, B. P. M., Weeren, P. R., Ederveen, A. G. H. & Barneveld, A. Influence of exercise on bone mineral density of immature cortical and trabecular bone of the equine metacarpus and proximal sesamoid bone. *Equine Veterinary Journal* **31**, 79–85 (2010).

35. Klintström, E., Smedby, Ö., Klintström, B., Brismar, T. B. & Moreno, R. Trabecular bone histomorphometric measurements and contrast-to-noise ratio in CBCT. *Dentomaxillofacial Radiology* **43**, 20140196 (2014).
36. Qiu, Y. *et al.* Bone microarchitectural parameters can detect oxytocin induced changes prior to bone density on mitigating bone deterioration in rabbit osteoporosis model using micro-CT. *BMC Musculoskeletal Disorders* **20**, 560 (2019).
37. Analyze 12.0: Bone Microarchitecture Analysis Manual. (2014).
38. Doube, M. Volume Fraction. *BoneJ* https://bonej.org/volumefraction.
39. Ding, M. Microarchitectural adaptations in aging and osteoarthrotic subchondral bone issues. *Acta Orthopaedica* **81**, 1–53 (2010).
40. Doube, M. Connectivity. *BoneJ* https://bonej.org/connectivity.
41. Fürst, A. *et al.* Effect of age on bone mineral density and micro architecture in the radius and tibia of horses: An Xtreme computed tomographic study. *BMC Vet Res* **4**, 3 (2008).
42. Bouxsein, M. L. *et al.* Guidelines for assessment of bone microstructure in rodents using micro–computed tomography. *Journal of Bone and Mineral Research* **25**, 1468–1486 (2010).
43. Doube, M. Anisotropy. *BoneJ* https://bonej.org/anisotropy.
44. *Clinical anatomy of the horse*. (Elsevier Mosby, 2005).
45. Alrtib, A. M., Philip, C. J., Abdunnabi, A. H. & Davies, H. M. S. Morphometrical Study of Bony Elements of the Forelimb Fetlock Joints in Horses. *Anat. Histol. Embryol.* **42**, 9–20 (2013).
46. Beccati, F. *et al.* Morphologic Radiographic Study of the Proximal Sesamoid Bones of the Forelimb in Thoroughbred Racehorses in Training. *Anat. Histol. Embryol.* **43**, 403–407 (2014).
47. Denoix, J.-M. Functional Anatomy of Tendons and Ligaments in the Distal Limbs (Manus and Pes). *Veterinary Clinics of North America: Equine Practice* **10**, 273–322 (1994).
48. Biewener, A. A. Muscle-tendon stresses and elastic energy storage during locomotion in the horse. *Comparative Biochemistry and Physiology Part B: Biochemistry and Molecular Biology* **120**, 73–87 (1998).
49. Relationship between muscle forces, joint loading and utilization of elastic strain energy in equine locomotion | Journal of Experimental Biology | The Company of Biologists. https://journals.biologists.com/jeb/article/213/23/3998/10063/Relationship-between-muscle-forces-joint-loading.
50. Merritt, J. S., Davies, H. M. S., Burvill, C. & Pandy, M. G. Influence of Muscle-Tendon Wrapping on Calculations of Joint Reaction Forces in the Equine Distal Forelimb. *Journal of Biomedicine and Biotechnology* **2008**, 1–9 (2008).
51. Harrison, S. M., Chris Whitton, R., Kawcak, C. E., Stover, S. M. & Pandy, M. G. Evaluation of a subject-specific finite-element model of the equine metacarpophalangeal joint under physiological load. *Journal of Biomechanics* **47**, 65–73 (2014).
52. Stoddart, M. J., Craft, A. M., Pattappa, G. & Gardner, O. F. W. *Developmental Biology and Musculoskeletal Tissue Engineering: Principles and Applications*. (Elsevier Science & Technology, 2018).

53. Parsons, F. G. Observations on Traction Epiphyses. *J Anat Physiol* **38**, 248–258 (1904).
54. Hall, B. K. *Bones and Cartilage: Developmental and Evolutionary Skeletal Biology*. (Elsevier Science & Technology, 2015).
55. Jahss, M. H. The Sesamoids of the Hallux: *Clinical Orthopaedics and Related Research* **NA;**, 88–97 (1981).
56. Cox, C. F., Sinkler, M. A. & Hubbard, J. B. Anatomy, Bony Pelvis and Lower Limb, Knee Patella. in *StatPearls* (StatPearls Publishing, 2021).
57. Gray, D. J. & Gardner, E. Prenatal development of the human knee and superior tibiofibular joints. *Am. J. Anat.* **86**, 235–287 (1950).
58. Fox, A., Wanivenhaus, F. & Rodeo, S. The Basic Science of the Patella: Structure, Composition, and Function. *J Knee Surg* **25**, 127–142 (2012).
59. Rida-Velasco, J. A. M. *et al.* Development of the human knee joint ligaments. 10.
60. Anderson, H. Histochemical Studies on the Histogenesis of the Knee Joint and Superior Tibio-Fibular Joint in Human Foetuses. *Acta anat.* **46**, 279–303 (1961).
61. Eyal, S. *et al.* On the development of the patella. *Development* **142**, 1831–1839 (2015).
62. Eyal, S., Rubin, S., Krief, S., Levin, L. & Zelzer, E. Common cellular origin and diverging developmental programs for different sesamoid bones. *Development* **146**, dev167452 (2019).
63. Sarin, V. K., Erickson, G. M., Giori, N. J., Bergman, A. G. & Carter, D. R. Coincident development of sesamoid bones and clues to their evolution. 7.
64. Small, K. M. & Potter, S. S. Homeotic transformations and limb defects in Hox All mutant mice. *Genes & Development* **7**, 2318–2328 (1993).
65. Ogden, J. A. Radiology of postnatal skeletal development. *Skeletal Radiology* **11**, 246–257 (1984).
66. Dharap, A. S., Al-Hashimi, H., Kassab, S. & Abu-Hijleh, M. F. Incidence and ossification of sesamoid bones in the hands and feet: A radiographic study in an Arab population. *Clin. Anat.* **20**, 416–423 (2007).
67. Sun, T. *et al.* Ossification timeline of sesamoid bones at metatarsophalangeal joints. *Anat Sci Int* **96**, 55–61 (2021).
68. Butler, J. A., Colles, C. M., Dyson, S. J., Kold, S. E. & Poulos, P. W. Metacarpophalangeal and metatarsophalangeal (fetlock) joints. in *Clinical Radiology of the Horse* 187–226 (Wiley Blackwell, 2017).
69. Firth, E. C. Fetal Ossification and Normal Joint Development. in *Equine Reproduction* (eds. McKinnon, A. O., Squires, E. L., Vaala, W. E. & Varner, D. D.) vol. 1 433–440 (Wiley-Blackwell, 2011).
70. Liley, H., Zhang, J., Firth, E. C., Fernandez, J. W. & Besier, T. F. Statistical modeling of the equine third metacarpal bone incorporating morphology and bone mineral density. *PLoS ONE* **13**, e0194406 (2018).
71. Babiarz, K. M. STRUCTURAL ADAPTATION OF EQUINE PROXIMAL SESAMOID BONES TO HIGH-SPEED EXERCISE. (University of Kentucky).
72. Stover, S. M. The epidemiology of Thoroughbred racehorse injuries. *Clinical Techniques in Equine Practice* **2**, 312–322 (2003).

VITA

1. Bachelor of Science, Auburn University, Dec. 2018
2. Graduate Research Assistant, University of Kentucky, Aug. 2019-Present
3. Cum Laude, Auburn University, Dec. 2018
4. A.M. Mangine, K.M. Babiarz, J.E. Davis, S.K. McLetchie, K.S. Garrett, C. Mok, B.C. Menarim, E.N. Adam, G. Zhang, J.G. Janes, L.A. Kennedy, J.N. MacLeod. Maturation of proximal sesamoid bones in Thoroughbred horses. *Journal of Equine Veterinary Science* 100(2021). ISSN 0737-0806. https://doi.org/10.1016/j.jevs.2021.103495.
5. Angela Maria Mangine